OXFORD

Cerebral Cortex, June 2016;26: 2832–2849

doi: 10.1093/cercor/bhw037
Advance Access Publication Date: 5 March 2016
Original Article

ORIGINAL ARTICLE

Cortical Structure Alterations and Social Behavior Impairment in p50-Deficient Mice

Sara Anna Bonini[1], Andrea Mastinu[1], Giuseppina Maccarinelli[1], Stefania Mitola[1], Marika Premoli[1], Luca Rosario La Rosa[1], Giulia Ferrari-Toninelli[1], Mariagrazia Grilli[2] and Maurizio Memo[1]

[1]Department of Molecular and Translational Medicine, University of Brescia, 25123 Brescia, Italy and [2]Laboratory of Neuroplasticity, Department of Pharmaceutical Sciences, University of Piemonte Orientale, 28100 Novara, Italy

Address correspondence to Sara Anna Bonini, Department of Molecular and Translational Medicine, University of Brescia, Viale Europa, 11, 25123 Brescia, Italy. Email: sara.bonini@unibs.it

Abstract

Alterations in genes that regulate neurodevelopment can lead to cortical malformations, resulting in malfunction during postnatal life. The NF-κB pathway has a key role during neurodevelopment by regulating the maintenance of the neural progenitor cell pool and inhibiting neuronal differentiation. In this study, we evaluated whether mice lacking the NF-κB p50 subunit (KO) present alterations in cortical structure and associated behavioral impairment. We found that, compared with wild type (WT), KO mice at postnatal day 2 present an increase in radial glial cells, an increase in Reelin protein expression levels, in addition to an increase of specific layer thickness. Moreover, adult KO mice display abnormal columnar organization in the somatosensory cortex, a specific decrease in somatostatin- and parvalbumin-expressing interneurons, altered neurite orientation, and a decrease in Synapsin I protein levels. Concerning behavior, KO mice, in addition to an increase in locomotor and exploratory activity, display impairment in social behaviors, with a reduction in social interaction. Finally, we found that risperidone treatment decreased hyperactivity of KO mice, but had no effect on defective social interaction. Altogether, these data add complexity to a growing body of data, suggesting a link between dysregulation of the NF-κB pathway and neurodevelopmental disorders pathogenesis.

Key words: cortical structure, neurodevelopmental disorders, NF-κB, $p50^{-/-}$ mice, social behavior

Introduction

The embryonic development of the cortex is a complex process controlled by a multitude of genes. Alterations in these regulatory genes can lead to cortical malformations, resulting in malfunction during postnatal life. Different cortical abnormalities are caused by mutations in key genes involved in different steps of cortical development, including abnormal neural proliferation, migration defects, or formation of circuits/synaptogenesis. The main diseases related to abnormal neurodevelopment are Down syndrome, schizophrenia, bipolar disorder, major depressive disorder, autism, and epilepsy.

Two master regulators in neurodevelopment are NF-κB and Notch proteins. Indeed, they are involved in cell proliferation and differentiation (Kovács et al. 2004; Lasky and Wu 2005), cell survival and death (Grilli and Memo 1999; Kucharczak et al. 2003; Mason et al. 2006), cell fate determination, and migration (Widera et al. 2006; Breunig et al. 2007; Gaiano 2008). In particular, during early stages of brain development, NF-κB is selectively

activated in neocortical neural progenitor cells to inhibit neuronal differentiation and maintain the progenitor cell pool (Methot et al. 2013). Also Notch pathway plays multiple roles in neurodevelopment including the regulation of neural stem cell proliferation, survival, self-renewal, specification of cell fate or differentiation, and apoptosis (Lasky and Wu 2005; Yoon and Gaiano 2005). Furthermore, Notch is involved in cortex cytoarchitecture formation and remodeling, since it regulates cortical neuron migration by interacting with Reelin-DAB1 signaling (Hashimoto-Torii et al. 2008). Notch is also essential for the maintenance of the neural stem/progenitor cell pool, as disruption of the Notch cascade leads to precocious neurogenesis and depletion of the germinal pool. More specifically, as neocortical neural stem cells are radial glia, Notch activation by ligand-expressing neurons or intermediate progenitors maintains radial glial capacity of self-renewal while inhibiting neurogenesis (Yoon et al. 2008).

Together, both Notch and NF-κB signaling pathways may potentially contribute, by a reciprocal crosstalk interaction, to regulate neurodevelopment in physiological and pathological conditions. Numerous cellular contexts have been described wherein interaction of Notch and NF-κB signaling pathways takes place (Osipo et al. 2008; Cao et al. 2010), but clear indications of their functional crosstalk in brain development and its potential relevance in CNS disorders still remain to be demonstrated (Ang and Tergaonkar 2007).

In previous studies, by using $p50^{-/-}$ mice, lacking the NF-κB p50 subunit, we demonstrated that a direct crosstalk between NF-κB and Notch does exist in the cortex and it plays a role in regulating cortical neuron structural plasticity. Moreover, we could show that the lack of p50 subunit resulted in Notch signaling hyperactivation in cortical neurons (Bonini et al. 2011).

$p50^{-/-}$ mice are viable and fertile, with no obvious developmental or histopathological abnormalities, but with in-depth analysis and aging they display several selective defects. Sha et al. (1995) reported an alteration in B lymphocyte response and in basal and specific antibody production. Kassed and Herkenham observed that $p50^{-/-}$ mice had reduced body weight compared with wild-type controls and showed functional defects in a number of sensorimotor tests. In particular, they demonstrated that $p50^{-/-}$ mice have a distinctive behavioral phenotype characterized by decreased anxiety-like responses, elevated exploratory behavior, and reduced tendency to establish dominant-subordinate relationships among cage mates (Kassed and Herkenham 2004). In addition, Kassed et al. (2002) demonstrated that $p50^{-/-}$ mice performed poorly in acquiring escape behavior in an active avoidance paradigm, concluding that absence of p50 negatively modulates learning ability. Finally, a dramatic impairment in hippocampal neurogenesis linked to a selective cognitive deficit in hippocampal-dependent spatial short-term memory was demonstrated in $p50^{-/-}$ compared with wild-type mice (Denis-Donini et al. 2008).

Now we hypothesize and investigate whether, due to the key role of NF-κB and Notch during neurodevelopment and to dysregulated Notch pathway in $p50^{-/-}$ mice, these mutant mice may present structural alterations in their cortex and associated behavioral defects.

Materials and Methods

Animals

Experiments were conducted in conformity with the European Communities Council Directive of 1986 (86/609/EEC) and approved by the Italian Ministry of Health, Animal care and use Committee of the University of Brescia. Animals were housed 2 to 3 per cage in a 12 h light/dark cycle (light phase: from 8:00 a.m. to 8:00 p.m.) with food and water available *ad libitum*. The cage size was 15 cm wide × 35 cm long × 12 cm deep. Temperature (22°C) and humidity (50 ± 10%) in the cage were automatically regulated by the Sealsafe Aero System by individually ventilated cages with EPA filters (Tecniplast Group, Italy). NF-κB $p50^{-/-}$ mice (B6;129P2-*Nfkb 1tm 1 Bal/J*) and wild-type mice (B6;129PF2) were purchased from The Jackson Laboratories (Bar Harbor, ME, USA). For cortical neurons migration and cortical layering analysis, postnatal day 2 (P2) mice were used. P2 mice used for experiments derived from different litters; they were obtained in our animal facility from mating mice. Each breeder male mouse was maintained in the same cage with a female mouse till litter birth; then male mouse was removed and replaced in mating cage after litter weaning. In all other experiments, wild-type (WT) and $p50^{-/-}$ (KO) age-matched mice (2–6 month old; weight = 25–35 g) were used. All the experiments were performed on male mice. Breeder mice were used only for mating, not for experiments.

Drug Treatment

For acute treatment, risperidone (Sigma-Aldrich) (0.03, 0.06, 0.125, 0.5, 1 mg/kg in a 10 mL/kg volume) or vehicle (0.9% NaCl) was administered via intraperitoneal injection 30 min before testing for both the open field and the social approach tests, according to previously reported data (Gould et al. 2011; Amodeo et al. 2014). For chronic treatment, mice were exposed to intragastric administration of 0.3 mg/kg risperidone or vehicle for 3 weeks. The dose was chosen on the basis of the acute treatment results. Finally, treated mice were tested for both the open field and the social approach tests.

Immunohistochemistry

Mouse brains were collected, fixed, cryoprotected, and coronally cryosectioned at 20 μm using standard methods. For immunolabeling, the following primary antibodies were used: mouse anti-Reelin (G10, 1:1000; GeneTex), rabbit anti-BLBP (ABN14, 1:300; Millipore), rat anti-CTIP2 (25B6, 1:250; Abcam), rabbit anti-CDP/Cux1 (M-222, 1:300; Santa Cruz Biotechnology), rabbit anti-Neurofilament-200 (N4142, 1:100; Sigma-Aldrich), mouse anti-Parvalbumin (PARV-19, 1:100; Sigma-Aldrich), rabbit anti-Neuropeptide Y (ab30914, 1:100; Abcam), rabbit anti-Somatostatin (H-106, 1:100; Santa Cruz Biotechnology). Primary antibodies were detected with the following secondary antibodies: goat anti-mouse CY3 (1:1000; Jackson ImmunoResearch), goat anti-rabbit Alexa Fluor 488 (1:400; Life Technologies), goat anti-rat DyLight 488 (1:100; KPL), goat anti-rabbit CY3 (1:1000; Jackson ImmunoResearch). For each section, images were acquired using a Zeiss Axiovert 200M epifluorescence microscope equipped with Plan Apochromat ×20/0.6 objective and ApoTome system. Images were automatically performed using the MosaiX and Z-Stack modules of the Zeiss AxioVision Software. For Neurofilament-200 images, a ZEISS LSM 510 META confocal laser scanning microscope (Zeiss) was used. For Reelin-BLBP images, a Zeiss Axio Vert.A1 microscope was used.

Quantification of Neurite Orientation

To perform a quantification of neurite orientation, a method similar to the Sholl analysis, commonly used for the quantification of branching in neurons (Sholl 1953), was applied. In particular, by using the ImageJ software, a grid formed by squares

(20 × 20 micron) was set on the cortex section images stained with the anti-Neurofilament-200 and placed with the vertical lines parallel to basal-apical orientation of neurites. Images acquired with the confocal microscope by using the ×40 objective were analysed. Somatosensory cortex of at least 3 animals for genotype was evaluated. All intersections between horizontal lines and nonvertically-oriented neurites were counted. In this way, a quantification of vertical orientation of neurites was obtained: higher the number of intersections, minor the vertical orientation of neurites.

Type-Specific Cell Counts

Immunohistochemistry for Brain Lipid Binding Protein (BLBP), a marker of radial glial cells, was performed on coronal brain sections of P2 WT and KO mice. BLBP-positive cells were counted in defined areas having a width of 200 μm and a height of 600 μm by ImageJ software. A minimum of 6 areas for each section was counted and a minimum of 3 animals for genotype was analysed. Data are expressed as mean ± S.E.M. of BLBP-positive cells per area.

Immunohistochemistry for Somatostatin, Parvalbumin, and Neuropeptide Y was performed on coronal brain sections of adult WT and KO mice. All 3 antibodies were used as markers of specific subtype of interneurons. Somatostatin, Parvalbumin, or Neuropeptide Y positive cells were counted in the somatosensory cortex, in defined areas having a width of 300 μm and a height of 1000 μm, by ImageJ software. A minimum of 6 areas for each section was counted and a minimum of 3 animals for genotype was analysed. Data are expressed as mean ± S.E.M. of positive cells per area.

Layer Thickness Measurement

Coronal brain sections of P2 WT and KO mice were processed by immunohistochemistry for cortical layer stratification analysis. The following antibodies were used: anti-CTIP2 and anti-CDP/Cux1. These antibodies are used as markers of specific cortical layers. In P2 mice brain, CTIP2-positive cells are normally suited in layers VI–V, while CUX1-positive cells in layers III–II.

Layer-specific markers represent also neuron type-specific markers. Hence, layer-specific patterns represent the radial distribution of distinct neuron types (Hevner 2007). COUP TF1-interacting protein 2 (CTIP2) positive cells are placed in the deep layers of the cerebral cortex and have been characterized as subcerebral projecting neurons: corticotectal neurons and corticospinal motor neurons (Arlotta et al. 2005; Chen et al. 2005, 2008). Cux1 homeodomain protein is expressed in layers II–III cortical neurons and positively regulate their dendritic growth and facilitate neuron ability to integrate information from multiple axonal inputs, enabling their specialized tasks (Cubelos et al. 2010).

To examine cortical layering, WT and KO sections immunolabeled for both CTIP2 and Cux1 proteins were analyzed with the Zeiss Axio Observer, and images were acquired with a Plan Apochromat ×20/0.6 objective. Then, the thickness of Cux1-positive cell layer, CTIP2-positive cell layer, and the distance between the 2 layers were measured. These measurements were obtained from different coronal brain sections and considering 3 defined points of each cortical hemisphere. Cortex thickness measurements were done using the ImageJ software.

Nissl Staining

Adult mice were anesthetized with chloral hydrate (400 mg/kg) and perfused transcardially with PBS, followed by 4% paraformaldehyde (PFA) in PBS. Brains were removed, postfixed overnight in 4% PFA/PBS, and cryoprotected in 30% sucrose/PBS. Brains were then cryosectioned at 20 μm and mounted on slides. Slides were passed through a graded series of ethanol solutions before being stained with a solution containing 0.5% cresyl violet acetate and 1% acetic acid. Slides were then dehydrated and mounted with DPX (Sigma-Aldrich).

Cortical Column Analysis

Cortical minicolumns were quantified using a semiautomatic image analysis as previously described (Buxhoeveden et al. 2000), with appropriate modifications to perform the analysis on mouse brain sections (as reported in Srivastava et al. 2012). Images of Nissl-stained brain sections were acquired by using a ×10 objective of an Olympus BX41 microscope. The following cortical areas were analysed in both cerebral hemispheres of at least 3 mice for genotype with the ImageJ software: anterior cingulate cortex (corresponding to bregma 1.70 and 1.94 mm) and somatosensory cortex (corresponding to bregma −1.28 and −1.64 mm). Images of cortical areas of interest were opened with the Image J software and automatically adjusted for brightness and contrast to reduce background. After setting the scale for pixel/micron conversion, a rectangular area having the size of a minicolumn region of interest (ROI) (width: 60 μm; height: 400 μm) was marked in layers II–IV, where columnar organization of the cortex is clearly defined. Up to 15 ROIs per section, placed at regular, nonoverlapping intervals across the image, were analysed. The image was processed to turn into a binary image, applying the Watershed algorithms to better define cell borders. The following parameters were measured in ROIs: cells density, cell spacing, total path length ratio (TPLR), and soma size. To calculate cell density, only cells with an area of 70–350 μm^2, and those that did not touch the edges of the defined column, were included in the quantification. The area range defined was set to restrict cell count to pyramidal neurons (excluding glia and interneurons) and to avoid multiple cells clusters. Cell spacing, defined as the total area of defined column minus the total area of cell somas, was calculated for each column. The TPLR provided information concerning the vertical orientation of the minicolumn: it results from the sum of the Euclidean distances between consecutive cells within a column divided by the linear depth of the column. The TPLR of a hypothetical column where all cells lie along a central line would be equal to 1.0, while TPLR of real columns is >1.0 (Buxhoeveden et al. 2000). Greater the TPLR value, minor the vertical organization of the minicolumn.

Western Blotting

For Reelin protein levels, protein extracts were prepared from cortical tissue extracted from WT and KO P2 mice. For other proteins, extracts were prepared from somatosensory cortical tissue, dissected from 400-μm-thick brain sections of WT and KO adult mice. Western blotting was performed using 10–12% SDS polyacrylamide precast gels (BIO-RAD Laboratories) with 15–30 μg of protein extracts loaded per lane. Protein transfer on nitrocellulose membrane was done by using the Trans-Blot Turbo Transfer System (BIO-RAD Laboratories). Nitrocellulose filters were incubated with primary antibodies raised against Reelin (G10, 1:1000; GeneTex), NeuN (A60, 1:1000; Chemicon), GFAP (G-A-5, 1:500; Sigma-Aldrich), GAD65 (GAD-6, 1:1000; abcam), GAD67 (1G10.2, 1:1000; Merck Millipore), Synapsin I (S193, 1:2000; Sigma-Aldrich), and GAPDH (6C5, 1:500; Merck Millipore) overnight at 4°C, followed by IRDye 800CW- or 680LT-conjugated

secondary antibodies (1:1500; LI-COR). To visualize bands, Odyssey Fc Imager was used. Densitometric analysis was performed using Image Studio Software (LI-COR), and each band was normalized to the GAPDH signal in each lane and expressed as percentage.

RNA Isolation

Total RNA was isolated from somatosensory cortical tissue, dissected from 400-μm-thick brain sections of WT and KO adult mice. To purify RNA, the RNeasy kit (Qiagen) was used and RNA digested with the RNase-Free DNAse set (Qiagen), according to the manufacturer's protocol. RNA quality of samples was tested by RNA electrophoresis to ensure RNA integrity. RNA was quantified by means of Quantus Fluorometer (Promega).

Quantitative real-time PCR

One or 2 μg of total RNA from WT and KO cortical tissue was transcribed into cDNA using murine leukemia virus reverse transcriptase (Promega) and oligo(dT) 15–18 as a primer (final volume: 50 μL). Parallel reactions containing no reverse transcriptase were used as negative controls to confirm the removal of all genomic DNA. Murine-specific primers were designed using the Primer3 software (http://frodo.wi.mit.edu) (Rozen and Skaletsky 2000) or as previously described (Sgadò et al. 2013). The oligonucleotide sequences of the primers used are as follow: GFAP forward primer 5′-ATT GCT GGA GGG CGA AGA A-3′, reverse primer 5′-CGG ATC TGG AGG TTG GAG AA-3′, vGLUT forward primer 5′-CAC AGA AAG CCC AGT TCA AC-3′, reverse primer 5′-CAT GTT TAG GGT GGA GGT AGC-3′, vGAT forward primer 5′-TCA CGA CAA ACC CAA GAT CAC-3′, reverse primer 5′-GTC TTC GTT CTC CTC GTA CAG-3′, GAD65 forward primer 5′-TCA ACT AAG TCC CAC CCT AAG-3′, reverse primer 5′-CCC TGT AGA GTC AAT ACC TGC-3′, GAD67 forward primer 5′-CTC AGG CTG TAT GTC AGA TGT TC-3′, reverse primer 5′-AAG CGA GTC ACA GAG ATT GGT C-3′, Parvalbumin forward primer 5′-TGC TCA TCC AAG TTG CAG G-3′, reverse primer 5′-GCC ACT TTT GTC TTT GTC CAG-3′, Neuropeptide Y forward primer 5′-TCA CAG AGG CAC CCA GAG-3′, reverse primer 5′-AGA GAT AGA GCG AGG GTC AG-3′, Somatostatin forward primer 5′-AGG ACG AGA TGA GGC TGG-3′, reverse primer 5′-CAG GAG TTA AGG AAG AGA TAT GGG-3′, β-ACTIN forward primer 5′-AGC CAT GTA CGT AGC CAT CC-3′, reverse primer 5′-CTC TCA GCT GTG GTGGTG AA-3′; dopaminergic D_2 receptor forward primer 5′-ACC TGT CCT GGT ACG ATG ATG-3′, reverse primer 5′-GCA TGG CAT AGT AGT TGT AGT GG-3′; 5-HT_{2A} receptor forward primer 5′-CAT TGC GGG AAA CAT ACT GGT-3′, reverse primer 5′-CCA GCA GCA TAT CAG CTA TGG-3′. Amplification and detection were performed with the ViiA7 Real Time PCR Detection System (Applied Biosystem); the fluorescence signal was generated by SYBR Green I. Samples were run in triplicate in a 12 μL reaction mix containing 6 μL 2× SYBR Green Master Mix (BIO-RAD Laboratories), 6 pmol of each forward and reverse primer, and 2 μL of diluted cDNA. The SYBR Green Master Mix includes ROX as passive reference. Each PCR experiment included serial dilutions of a positive control for the construction of the calibration curve, a positive and a negative DNA sample, and water blanks. The PCR program was initiated by 10 min at 95°C before 40 cycles, each one of 1 s at 95°C and 30 s at 60°C. A subsequent dissociation curve analysis verified the products specificity. Gene expression levels were normalized to β-actin expression, and data are presented as the fold change in target gene expression in KO cortical tissue normalized to the internal control gene and relative to WT cortical tissue. Results were estimated as Ct values; the Ct was calculated as the mean of the Ct for the target gene minus the mean of the Ct for the internal control gene. The Ct represented the mean difference between the Ct of KO minus the Ct of WT cortical tissue. The *N*-fold differential expression in the target gene of KO compared with WT cortical tissue was expressed as $2^{-\Delta\Delta Ct}$. Data analysis and graphics were performed using GraphPad Prism 5 software and were the results of 6 mice per group (WT and KO cortical tissue), each sample run in triplicate for each gene.

Behavioral Analysis

Open Field Exploration

After being acclimated to the procedure room for at least 10 min, each of WT or KO mouse (age-matched adults, 2–4 month old, 10 per group) was individually videotaped during a 5-min exploration session in a 40 × 40 cm Plexiglas open field activity box. Mice were placed in the center of the arena at the beginning of the test period. Their movement around the arena was recorded by a portable video camera vertically mounted 1.5 m above and remotely controlled by the experimenter. The Plexiglas box was cleaned after each individual test session to prevent subsequent mice from being influenced by odors deposited by previous mice. Testing was performed under normal room lights, during the light phase of the circadian cycle, between 09:30 and 17:30 h. Locomotor activity was recorded and total distance travelled, average speed, and total time mobile were analysed and automatically scored with ANY-maze software.

Reciprocal Social Interaction

Fine-grained measures of interactions between pairs of adult mice placed together in standard cages or arenas provide the most detailed insights into reciprocal social interactions (Silverman et al. 2010). For this behavioral analysis, at least 10 pairs of 2- to 4-month-old male, age-matched, mice for each genotype were used. The experimental mice were individually housed during 48 h preceding the behavioral test. For the test, after a period of acclimation of 10 min into their cage in a quiet and dim experimental room, subjects were exposed to an age-, sex-, and strain-matched unfamiliar subject (intruder subject) for 10 min. The 10-min social test was videorecorded and later analyzed by the operator on the video collected with the IC Capture software (VisionLink). Duration and frequency of anogenital sniffing, nose to nose sniffing, wrestling, cage exploring, self-grooming, following, mounting, pushing past each other with physical contact, climbing were measured as well as the first contact latency. During the test, the operator remained in an adjacent room, separated with a dark sliding door from the test room.

Social Approach

To evaluate the mice social approach, a "three-chambered" apparatus was used (Yang et al. 2011). It consists of a rectangular three-chambered box made of clear polycarbonate; each chamber measures 26 cm (length) × 35 cm (width) × 20 cm (height). The dividing walls have small openings (10 cm width × 10 cm height) that allow access into each chamber and that can be opened or closed only by the operator. The central chamber is the start location. For this behavioral analysis, 10–12 age-matched mice (4–6 month old) for each genotype were used. A period of acclimation of 10 min into their cage in a quiet and dim experimental room always preceded the test. The test is composed of 4 phases, 10 min each. Phase I: habituate the subject mouse to the center chamber; during this phase, the mouse is gently placed into the central chamber with the two doorways closed and let quite to familiarize with the location. Phase II: habituate the mouse to all the three chambers; during this phase, the two doorways are

open, so the mouse can freely circulate into the entirely empty three chambers. Chamber time data from phase II provide readouts that confirm whether room cues are well balanced; indeed no side preference as well as no locomotor problems of the animal has to emerge. Phase III: test for sociability; during this phase, the two doorways are open and in one lateral chamber a novel mouse (social stimulus, represented by an age- and genotype-matched mouse) is placed under an inverted wire pencil cup, while in the other lateral chamber a nonsocial novel object (an identical inverted wire pencil cup) is set. Sociability is defined as the subject mouse spending more time in the chamber containing the novel target mouse than in the chamber containing the inanimate novel object. Phase IV: test preference for social novelty; during this phase, the two doorways are open and in one lateral chamber the mouse used also in the previous phase (novel mouse 1) is placed, while in the other lateral chamber a second novel mouse (novel mouse 2, represented by an age- and genotype-matched mouse) is placed, both mice set under an inverted wire pencil cup. Preference for social novelty is defined as more time spent in the chamber with novel mouse 2 than time in the chamber with novel mouse 1. The 40-min social test was videorecorded and later analysed by the operator on the video collected with the IC Capture software. The following parameters were measured for the analysis: time spent in each compartment, number of entries into each compartment (exploratory locomotion index), time spent sniffing the novel target mouse, time spent sniffing the novel object, and time spent sniffing the second novel mouse (for social memory evaluation). During the test, the operator remained in an adjacent room, separated with a dark sliding door from the test room.

Statistical Analysis

Statistical analysis was performed by GraphPad Prism 5 software. For the social approach test with the three-chambered apparatus, both the Two-way analysis of variance (ANOVA) followed by the Bonferroni post-test analysis and the Two-way ANOVA followed by the Sidak's multiple comparison test were used. For the acute risperidone treatment, the One-way ANOVA followed by the Dunnett's multiple comparison test was performed. For the dopaminergic and serotoninergic receptors expression levels analysis, One-way analysis of variance and Bonferroni's multiple comparison test was used. Unpaired Student's *t*-test (WT vs. KO) was used for all other experiments, with statistical significance level set at $P < 0.05$. Data are presented as means ± S.E.M.

Results

Number of Radial Glial Cells and Reelin Expression Level Are Increased in p50$^{-/-}$ Mouse Cortex

At first, we hypothesized that an unbalance of NF-κB and Notch signaling pathways during crucial steps in neurodevelopment could lead to alteration in cerebral cortex formation. In particular, we focused on two proteins with a major role in corticogenesis: BLBP, a marker of radial glial cells during development, and Reelin. BLBP is a nervous system-specific member of the large family of hydrophobic ligand-binding proteins, and it is exclusively expressed in radial glia and astrocytes during development throughout the CNS (Feng et al. 1994; Hartfuss et al. 2001). Interestingly, BLBP is a direct target of Notch signaling in radial glial cells; indeed, it has been demonstrated that a binding site for the Notch effector CBF1 is essential for all *Blbp* gene transcription in radial glia (Anthony et al. 2005). Reelin is a large secreted glycoprotein that guide neuronal migration and proper positioning of neurons in the cerebral cortex and cerebellum (Caviness and Rakic 1978; D'Arcangelo et al. 1995). It has already been demonstrated that a crosstalk between Reelin and Notch exists during cortical development. The two pathways indeed interact in neocortical neurons to regulate migration and laminar positioning (Gaiano 2008; Hashimoto-Torii et al. 2008). Furthermore, both Notch and Reelin receptors are expressed in radial glia, and activation of both pathways promotes radial glial character, including expression of the radial glial marker BLBP (Gaiano et al. 2000; Hartfuss et al. 2003; Keilani and Sugaya 2008).

To evaluate the last stage of cortical cell migration, WT and KO mice cortex was analysed in terms of BLBP and Reelin expression at postnatal day 2 (P2). An immunohistochemistry was performed to evaluate the localization pattern and expression of the two proteins. As expected, Reelin staining was found in the Cajal–Retzius layer, the most superficial cortical layer, both in WT and in KO mice cortex (Fig. 1*A*). Conversely, as expected, BLBP staining appeared widespread throughout the whole cortex, both in WT and in KO mice (Fig. 1*A*). No significant differences between WT and KO mice emerged for Reelin and BLBP localization or immunohistochemical pattern.

BLBP$^+$ cells were counted in both WT and KO mice brain sections, selecting a cortical area of 200 × 600 µm (width × height). As shown in Figure 1*B*, BLBP$^+$ cells were significantly increased in KO compared with WT cortex, with cell numbers per area being 14.76 ± 0.41 for WT and 18.26 ± 0.46 for KO mice, respectively (mean ± S.E.M, $P < 0.0001$). Due to the limited area of localization of the Reelin-expressing cells and to the secreted nature of this protein, Reelin expression levels were analyzed by western blotting. It emerged that also Reelin levels were increased in KO mice cortex compared with WT. As shown in Figure 1*C*, Reelin protein level (normalized to GAPDH signal, %) resulted in 103.5 ± 5.76 and 141.9 ± 15.03 for WT and KO mice, respectively (mean ± S.E.M., $P < 0.05$). Altogether these results demonstrate that both the number of BLBP$^+$ (radial glial cells) and Reelin expression levels are upregulated in cortices of P2 mice deficient in NF-κB p50 subunit, compared with their WT counterpart.

Cortical Layering in p50$^{-/-}$ Mice

The neocortex of mammals is organized in six layers, generated in an inside-out pattern (Marin-Padilla 1978) and contains two major types of projection neurons. The vast majority (~80%) are glutamatergic (excitatory) neurons extending their long axon into the ipsilateral or controlateral cortex (cortico-cortical neurons, located in layers II/III) or toward subcortical regions (cortico-fugal neurons, located in layers V/VI). The remainder (~20%) are GABAergic local circuit neurons (inhibitory interneurons) that establish synaptic contacts with excitatory neurons located in their proximity (Molyneaux et al. 2007). Alterations in cortical cells migration and differentiation during neurodevelopment may affect cortical layering (Rakic 1988; Moon and Wynshaw-Boris 2013).

To check whether p50$^{-/-}$ mice display abnormalities in cortex organization, we analyzed cortical layering in P2 mice, when neurogenesis and migration have primarily subsided (Munji et al. 2011). Layer-specific markers can be particularly useful for studying malformations of cortical development involving defects of neuron-type specification or differentiation, as well as altered laminar distribution (Hevner 2007). Two antibodies were used as layer-specific markers: Cux1, for layers III–II, and Ctip2, for layers VI–V. After immunolabeling, brain sections were

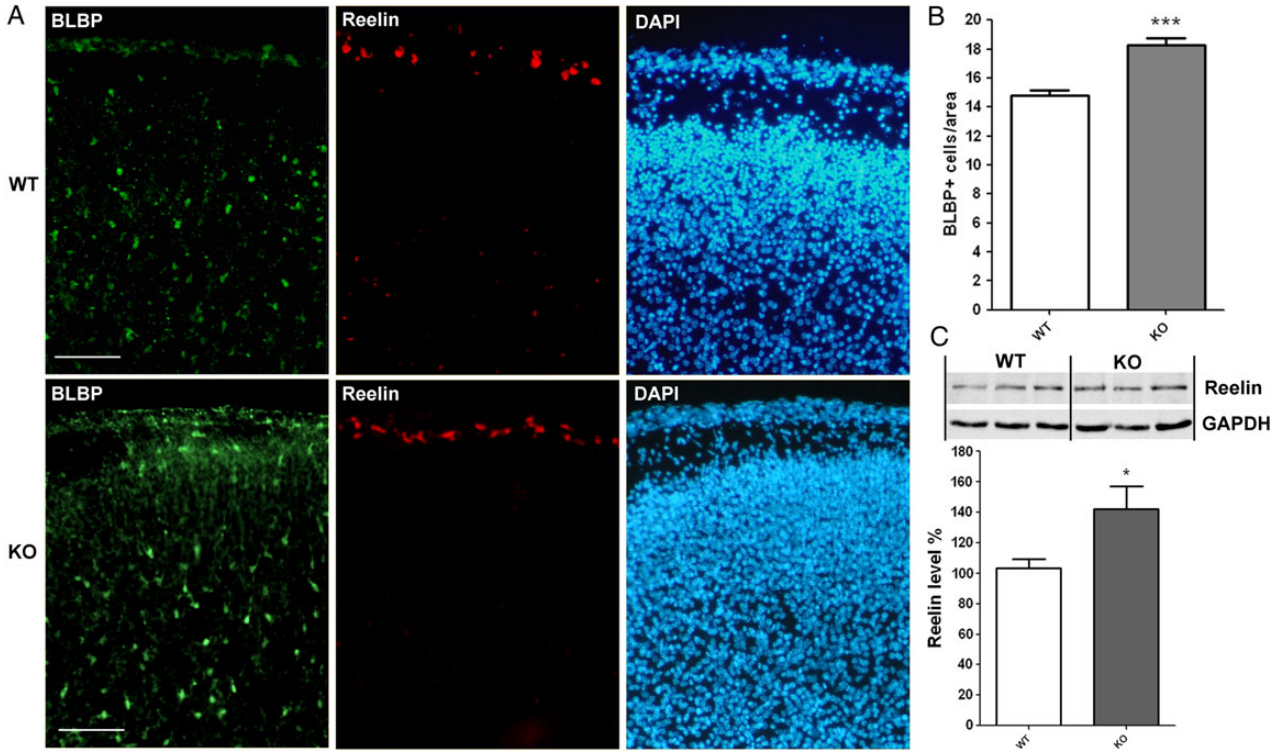

Figure 1. Radial glial cells and Reelin expression are increased in P2 $p50^{-/-}$ mice cortex. (*A*) Representative images of cortical sections from P2 wild-type (WT) (upper panels) and $p50^{-/-}$ (KO) (lower panels) mice stained with anti-Reelin (in red) and anti-BLBP (radial glial cells marker, in green) antibodies. Also nuclear DAPI staining (in blue) is reported. Scale bar, 100 µm. (*B*) Graphic representation of the number of $BLBP^+$ cells per area in WT and KO mice cortex. Data showed an increase in $BLBP^+$ cells in KO compared with that in WT mice cortex and are expressed as mean ± S.E.M. ***$P < 0.0001$ versus WT. (*C*) Upper panel: representative immunoblot of WT and KO P2 mice cortex lysates using anti-Reelin and anti-GAPDH antibodies. Graph: graphic representation of the densitometric analysis of Reelin expression levels measured by western blotting in WT and KO cortex. Data are normalized to the GAPDH signal and expressed as % mean ± S.E.M. *$P < 0.05$ versus WT.

visualized. At first, section analysis revealed no major differences between WT and KO cortical layer organization, with a comparable staining of both Cux1 and Ctip2 markers throughout the cortex and no abnormal laminar organization of KO cortex. Subsequently, a measurement of the Cux1- and Ctip2-positive cells layer thickness was performed, by comparing similar coronal WT and KO sections and measuring layer thickness in three different regions of the cortex: apical (A), intermedial (B) and medial (C) (Fig. 2). The analysis revealed no significant differences in the thickness of Cux1-positive cells layer in all the points of measurement [(A) mean ± S.E.M.: 438.4 ± 25.88 µm and 510.0 ± 46.59 µm; (B): 589.1 ± 37.75 µm and 664.0 ± 43.70 µm; (C): 613.7 ± 33.15 µm and 735.1 ± 53.01 µm for WT and KO mice, respectively]. On the contrary, the analysis of Ctip2-positive cell layer reported a significant increase in KO cortical layer thickness in all three regions of measurement [(A) mean ± S.E.M.: 454.2 ± 28.97 µm and 612.4 ± 38.64 µm; (B): 300.2 ± 11.64 µm and 471.9 ± 43.92 µm; (C): 331.3 ± 15.22 µm and 533.6 ± 46.91 µm for WT and KO mice, respectively; $P < 0.01$]. Also the distance between the two layers was measured, but no significant differences were reported [(A) mean ± S.E.M.: 164.0 ± 21.56 µm and 140.7 ± 23.62 µm; (B): 134.1 ± 28.73 µm and 92.88 ± 32.19 µm; (C): 195.4 ± 31.09 µm and 114.8 ± 25.00 µm for WT and KO mice, respectively]. Finally, total cortical thickness was measured. It emerged that the cortex of $p50^{-/-}$ mice is increased in thickness compared with wild-type mice (mean ± S.E.M.: 1073 ± 31.44 µm and 1294.9 ± 50.42 µm for WT and KO mice, respectively; $P < 0.001$). Altogether, in the presence of proper laminar organization, a specific increase in layers V–VI thickness was present at P2 in $p50^{-/-}$ mice cortex.

Abnormal Cortical Organization in the $p50^{-/-}$ Adult Mice SS Cortex

The "minicolumns," vertical columnar units of the neocortex, are anatomical and functional basal units of the neocortex (Mountcastle 1957, 1997) which are identified in all regions of the cortex and in all mammalian species (Casanova et al. 2006). The minicolumnar core comprises radially oriented arrays of pyramidal projection neurons.

To examine the cytoarchitecture of $p50^{-/-}$ adult mice, Nissl staining was performed on coronal brain slices taken from age-matched KO and WT mice, and the columnar organization in the somatosensory (SS) cortex of these mice was analyzed. The SS cortex was chosen for the analysis since in previous studies we found increased and altered expression pattern of both Notch1 receptor and its ligand Jagged1 in such area of P1 KO mice cortex (Bonini et al. 2011). To assess region specificity, we analysed the cingulate gyrus (CG) as an internal control.

We first examined gross anatomical structure of mice brains, but no significant differences were observed in both brain weight and shape between WT and KO mice (data not shown). Using previously examined methodology (Buxhoeveden et al. 2000), following appropriate modifications to perform the analysis on mouse brain sections (as reported in Srivastava et al. 2012), the number of cells within a defined column was evaluated. As previously reported (Srivastava et al. 2012), disruption of columnar organization can be detected by an altered number of cells within these defined columns. The overall cell number per minicolumn resulted in increased KO versus WT mice SS cortex (data not

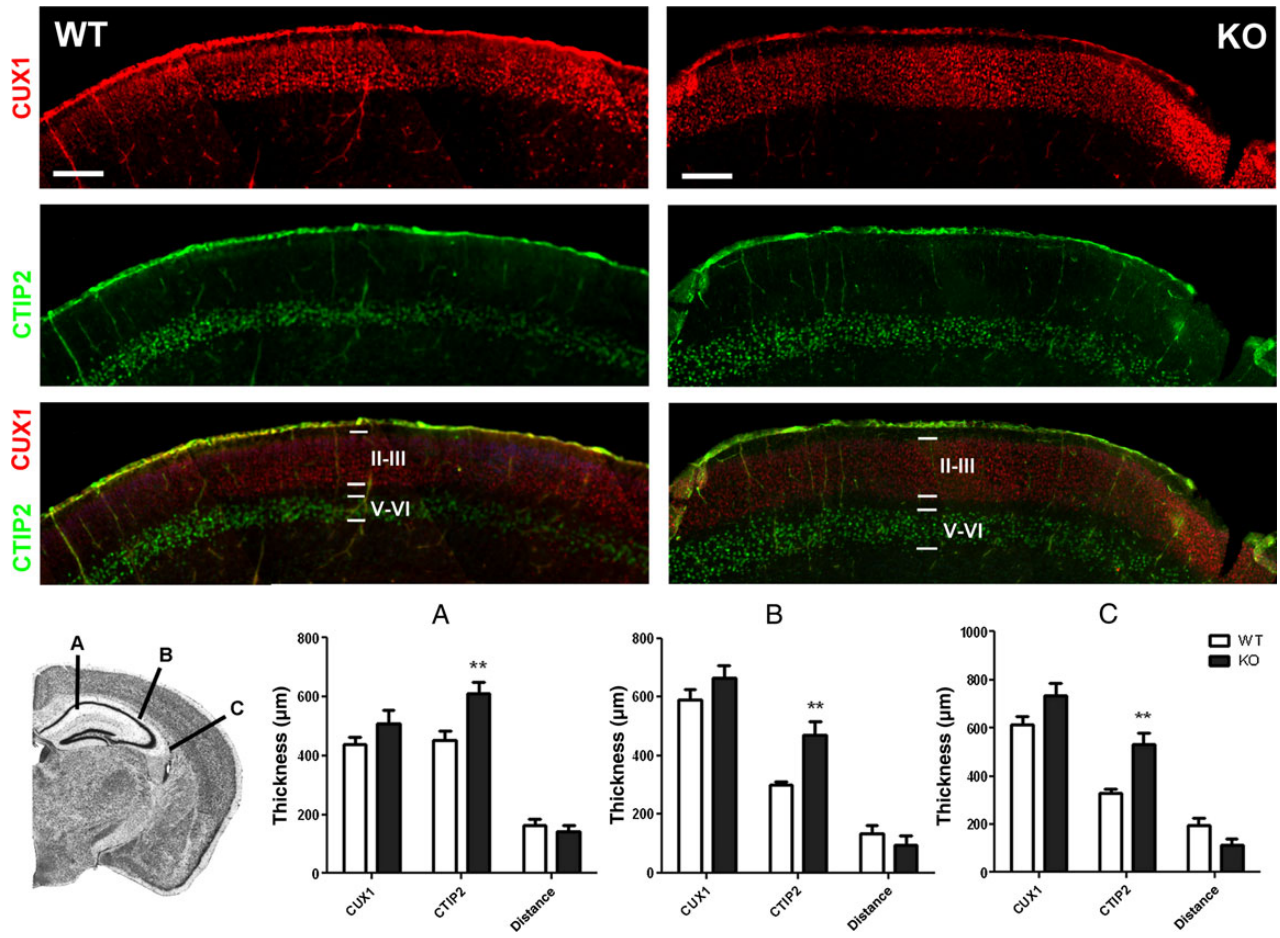

Figure 2. Increase in CTIP2 layer thickness in P2 p50$^{-/-}$ mice cortex. Upper panels, representative Axiovert 200 microscope images of a cerebral cortex area from P2 WT and KO mouse brain sections stained with anti-Cux1 (red), anti-CTIP2 (green) antibodies. Scale bar, 400 μm. Inset, Scheme of a P2 brain section with the indication (black marks with letters) of the three points of layer thickness measurements. As shown in the representative images, the CTIP2-positive cell layer thickness is increased in KO compared with WT mice cortex. Indeed, as shown in the graphic representation of the CTIP2^{+} and Cux1^{+} cells layer thickness and the distance between the two layers analysis, it emerged a significant increase in all the three points of measurement (*A*, *B*, and *C*). Data are expressed as mean ± S.E.M. In *A*, $^{**}P = 0.006$ versus WT; in *B*, $^{**}P = 0.002$ versus WT; in *C*, $^{**}P = 0.001$ versus WT.

shown). Subsequent analysis including only cells with an area of 70–350 μm^2 (pyramidal neurons) revealed an increase in cell density within a defined column in the SS cortex of KO versus WT mice (mean ± S.E.M., 20.72 ± 0.59 and 24.82 ± 0.66 for WT and KO mice, respectively; $P < 0.0001$), as reported in Figure 3A. Cell spacing, referred to as the total area of defined column minus the total area of somas within a defined column of the SS area, was also analyzed. This parameter showed a significant decrease for KO versus WT mice (mean area [mm^2] ± S.E.M., 21.73 ± 0.07 for WT; 21.28 ± 0.08 for KO; $P < 0.0001$). As a consequence, KO SS cortex displays less neuropil space, regarded as the synaptically dense area composed mostly of axons, dendrites and cell processes. The analysis of the total path length ratio (TPLR), a measurement of linearity of cell column, also revealed an increase in SS cortex columns of KO versus WT mice (mean ± S.E.M., 1.32 ± 0.02 for WT; 1.54 ± 0.02 for KO; $P < 0.0001$) (Fig. 3A). Conversely, there were no significant differences between WT and KO in SS cortex cell soma size (mean area [μm^2] ± S.E.M., 109.1 ± 1.32 for WT; 109.4 ± 1.35 for KO) (Fig. 3A). In Figure 3C, representative minicolumn binarized images of WT and KO SS cortex depict the increased average cell density per column with a reduction of vertical organization for pyramidal neurons in KO compared with WT mice. A parallel analysis of the same column parameters was performed on CG (Fig. 3B). In this cortical area, no difference between WT and KO cortical minicolumns emerged in terms of cells density (mean ± S.E.M., 23.50 ± 0.69 for WT; 21.98 ± 0.57 for KO), cell spacing (mean area [mm^2] ± S.E.M., 21.15 ± 0.10 for WT; 21.32 ± 0.08 for KO), TPLR (mean ± S.E.M., 1.417 ± 0.03 for WT; 1.361 ± 0.02 for KO), and soma size (mean area [μm^2] ± S.E.M., 121.2 ± 2.59 for WT; 123.3 ± 1.33 for KO).

Altogether, these data demonstrate that p50$^{-/-}$ mice exhibit SS cortex-specific alterations in columnar organization, with an increase in cell density, a reduction in neuropil space, and a loss of linearity in the vertical organization of the columns.

Characterization of Cortical Cell Subtypes in Adult Mice SS Cortex

Due to the increased cell density in the SS cortex of KO mice, a subsequent analysis aimed at identifying and quantifying changes in specific cellular subtypes in this cortical area was performed.

At first, protein levels of NeuN (neuron-specific nuclear protein, used as neuronal marker), GFAP (glial fibrillary acidic protein, used as marker of glial cells), GAD65 (the 65 kDa isoform of the enzyme glutamate decarboxylase, which catalyzes the

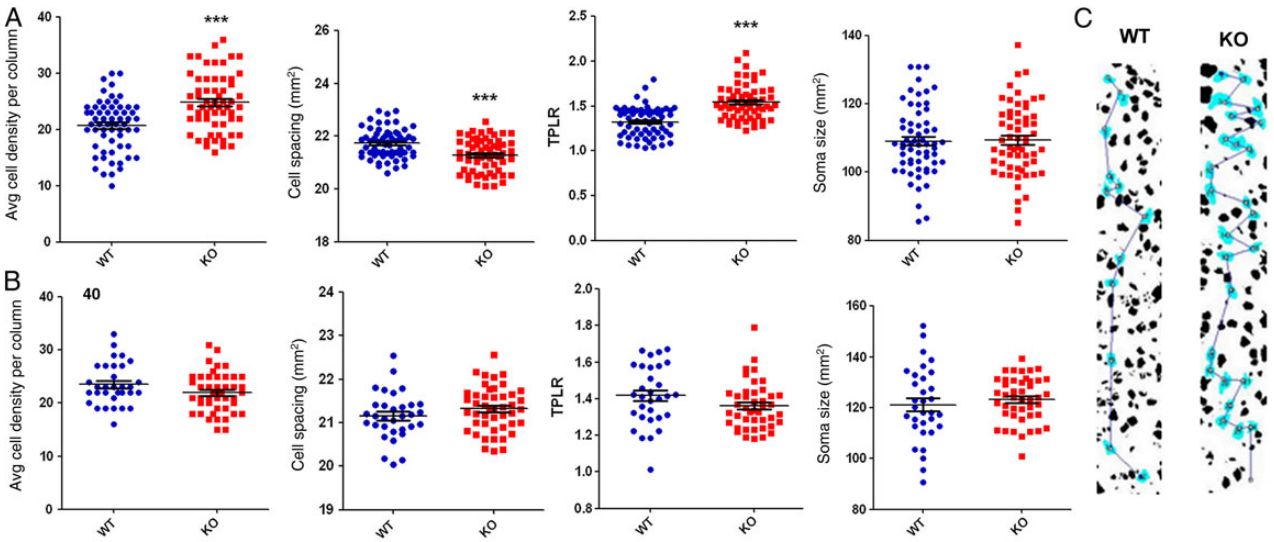

Figure 3. Abnormal columnar organization in the adult p50$^{-/-}$ mice SS cortex. (*A*) Graphic representation of data obtained from the minicolumn analysis in WT (blue points) and KO (red squares) somatosensory (SS) cortex. The following parameters were measured and reported in the graphs (from left to right): the average cell density per column, cell spacing, TPLR, and soma size. From the analysis, it emerged a significant increase in the average cell density per column (***$P < 0.0001$), a significant decrease in cell spacing (***$P < 0.0001$), a significant increase in TPLR (***$P < 0.0001$), but equal cells soma size in KO compared with WT SS cortex minicolumns. (*B*) Graphic representation of data obtained from the minicolumns analysis in WT (blue points) and KO (red squares) cingulate cortex (CG). From the analysis, it emerged no changes in all the parameters measured. (*C*) Representative minicolumn binarized images from WT (left) and KO (right) SS cortex. Blue cells are soma size-selected pyramidal neurons, and the blue line connecting them is TPLR. Average cell density per column resulted an increase for the SS cortex of KO mice compared with WT, but with a reduction in vertical organization (TPLR increase).

formation of GABA from glutamate), and GAD67 (the 67 kDa isoform of the enzyme glutamate decarboxylase) were evaluated by western blotting. As shown in Figure 4A, NeuN, GFAP, and GAD65 protein levels were all significantly increased in SS cortex of KO compared with that of WT mice (mean ± S.E.M., NeuN: 101.5 ± 5.24 for WT, 127.4 ± 9.63 for KO; GFAP: 100.0 ± 4.05 for WT, 131.5 ± 10.08 for KO; GAD65: 100.0 ± 7.54 for WT, 140.5 ± 12.20 for KO, $P < 0.05$ vs WT). GAD67 expression levels were also increased in KO SS cortex, but such increase did not reach statistical significance (mean ± S.E.M., 100.0 ± 8.40 for WT, 117.5 ± 10.36 for KO, $P = 0.20$).

Furthermore, to analyze the transcriptional activity of SS cortical cells, quantitative real-time PCR (QRT-PCR) analysis was also performed for vGLUT (vesicular glutamate transporter) for glutamatergic neurons, vGAT (vesicular GABA transporter) for GABAergic neurons, GFAP for glial cells, GAD65 and GAD67 for GABA-synthesizing neurons. As reported in Figure 4B, the relative expression levels of all markers remain unchanged between WT and KO mice.

Based on these results, we suggest that the increased cell density observed in the SS cortex of p50$^{-/-}$ mice may not be restricted to a specific cellular phenotype, but rather involve glutamatergic and GABAergic neurons and even glial cells, with no apparent change in their transcriptional activity between WT and KO mice.

In addition, different subtypes of interneurons were analysed and quantified in KO and WT mice SS cortex. Indeed, an unbalance between the glutamatergic and the GABAergic neuronal component of the cortex is a feature of several neurodevelopmental disorders, such as autism, schizophrenia, and epilepsy, characterized by alterations in the cortex cytoarchitecture and minicolumns abnormalities (Sgadò et al. 2013). Immunohistochemistry with antibodies anti-Somatostatin (SOM), anti-Parvalbumin (PARV), and anti-Neuropeptide Y (NPT Y) was performed on adult WT and KO brain section. SOM-, PARV-, and NPT Y-positive cells were counted in both WT and KO mice SS cortex, selecting a cortical area of 300 × 1000 μm (width × height). As shown in Figure 5A–D and B–E, both SOM- and PARV-positive cells resulted a significant decrease for KO mice SS cortex compared with WT. In particular, for SOM-positive cells, the mean cell number per area was 7.27 ± 0.29 for WT and 3.53 ± 0.17 for KO ($P < 0.0001$), whereas for PARV-positive cells 6.92 ± 0.26 for WT and 4.89 ± 0.23 for KO, respectively ($P < 0.0001$). On the other hand, NPT Y-positive cells remain unchanged between WT and KO mice SS cortex, with a mean cell number per area of 2.75 ± 0.18 and 3.03 ± 0.19 for WT and KO mice, respectively (Fig. 5C–F).

The same interneuron classes were analysed also by quantitative RT–PCR by using specific primers for SOM, PARV, and NPT Y on mRNA from SS cortex. Data obtained from QRT–PCR revealed a significant decrease in transcription for SOM (Fig. 5G), but not for PARV and NPT Y (Fig. 5H,I) (mean ± S.E.M., SOM: 1.04 ± 0.14 for WT, 0.33 ± 0.06 for KO, $P < 0.001$; PARV: 1.00 ± 0.03 for WT, 1.04 ± 0.01 for KO, $P = 0.22$; NPT Y: 1.00 ± 0.04 for WT, 0.96 ± 0.02 for KO, $P = 0.30$).

These results suggest that, despite a general increase in cell density in the SS cortex of KO mice, some specific subclasses of interneurons, namely the SOM- and PARV-expressing cells, are significantly reduced.

Altered Neurite Orientation in p50$^{-/-}$ Mice SS Cortex

The abnormal cortical structure observed in p50$^{-/-}$ adult mice SS cortex, and in particular alterations in columnar organization and increased cell density, led us to investigate neuron branching and synaptic net connections in cortical tissue. An immunohistochemistry analysis using an anti-Neurofilament-200 antibody to stain neurons was performed on WT and KO brain sections. As shown in representative images in Figure 6A, marked difference in neurite orientation of cortical neuron was observed in WT versus KO SS cortex. Indeed, while neurites of WT neurons

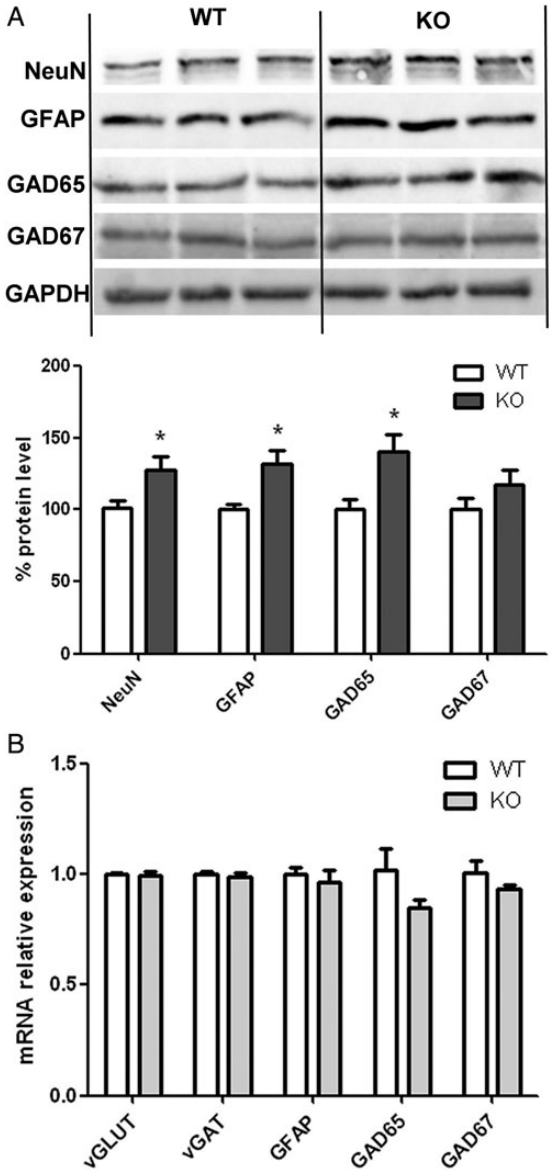

Figure 4. Cortical cells characterization in adult mice SS cortex. (*A*) Upper panel: representative immunoblots of WT and KO mice SS cortex lysates using anti-NeuN, anti-GFAP, anti-GAD65, anti-GAD67, and anti-GAPDH antibodies. Graph: Graphic representation of protein level analysis of NeuN (neuronal marker), GFAP (glial cells marker), GAD65, and GAD67 (GABAergic neurons markers) evaluated by western blotting. Data are expressed as mean ± S.E.M., normalized to GAPDH. NeuN, GFAP, and GAD65 resulted a significant increase for KO compared with WT SS cortex (*$P = 0.046$ for NeuN, *$P = 0.012$ for GFAP, *$P = 0.018$ for GAD65). (*B*) Graphic representation of QRT–PCR data obtained from RNA extracted from WT and KO SS cortex. Data (mean ± S.E.M.) are expressed as fold change of target gene expression in WT and KO cortex, normalized to the internal standard control gene (Actin). The following gene expressions were evaluated: vGLUT (for glutamatergic neurons), vGAT (for GABAergic neurons), GFAP (for glial cells), GAD65 and GAD67 (for GABA-synthesizing neurons). None of these transcripts showed a significant change in KO compared with WT mice.

had similar radial orientation from basal to apical cortical layers, in KO mice neurites lost their ordered orientation and were arranged in a disorganized pattern. Neurite orientation was quantified as reported in the Material and Method section. From this analysis, a significant increase emerged in the number of intersections in KO compared with WT mice somatosensory cortex (mean ± S.E.M.: 102.0 ± 5.686 and 136.7 ± 1.764 for WT and KO mice, respectively; $P < 0.005$). These data indicate that in p50 KO somatosensory cortex neurites lose their ordered basal–apical orientation typical of WT mice.

This observation is consistent with previously published data suggesting a role for Notch pathway in neurite process orientation during corticogenesis (Hashimoto-Torii et al. 2008), as well as with our previous data in primary cultures of cortical neurons (Bonini et al. 2011). Synapsins are important for the fine tuning of synaptic transmission (De Camilli et al. 1983; Fassio et al. 2011) and are considered key actors of synapse function and plasticity (Cesca et al. 2010). Among them, Synapsin I is a phosphoprotein localized in the membrane of synaptic vesicles. To analyze synaptic connections in SS cortex of WT and KO mice, Synapsin I expression levels were evaluated by western blotting. As shown in Figure 6*B* (upper panel), the anti-Synapsin I antibody recognized both Synapsin Ia and Synapsin Ib, with molecular weights of 80 and 77 kDa, respectively. As reported in the graph, a remarkable decrease in Synapsin I levels was observed in the SS cortex of KO compared with WT mice (mean ± S.E.M., 100.0 ± 9.29 for WT, 59.89 ± 6.30 for KO; $P < 0.005$), suggesting a reduction in synaptic connections in the absence of p50 subunit.

Increased Exploratory Activity and Reduced Social Interaction in p50$^{-/-}$ Mice

Based on the observed alterations in SS cortical cytoarchitecture in the p50$^{-/-}$ mice, we then investigated their behavioral phenotype and in particular their social attitude. Similar alterations in columnar cortical organization and cell plasticity (Srivastava et al. 2012), as well as imbalance between cell-type expression in cortex (Sgadò et al. 2013), have been previously reported in mouse models with social impairment.

At first, we tested both wild-type and p50$^{-/-}$ mice in the open field test, to evaluate their locomotion and exploratory activity. As previously described (Kassed and Herkenham 2004; Denis-Donini et al. 2008), p50$^{-/-}$ mice showed increased exploratory behavior compared with WT animals, with a significant increase in total distance travelled (mean [m] ± S.E.M., 8.11 ± 0.61 for WT; 16.74 ± 1.77 for KO; $P < 0.01$), average speed (mean [m/s] ± S.E.M., 0.027 ± 0.002 for WT; 0.056 ± 0.005 for KO; $P < 0.01$), and total mobile time in the 5 min test (mean [s] ± S.E.M., 178.1 ± 19.13 for WT; 253.6 ± 9.86 for KO; $P < 0.01$) (Fig. 7A).

To determine whether p50$^{-/-}$ mice display impaired sociability, we measured the tendency of a subject mouse to approach another unfamiliar mouse by means of the "three-chambered apparatus". Briefly, after 10 min of habituation of the "test" mouse to the social approach arena, and another 10 min of "environment exploration", a "social stimulus", namely a sex-, genotype-, and age-matched mouse (the "novel mouse") was placed within a wire cup on one side of the social approach arena, while a non-social stimulus (an identical wire cup, called the "novel object") was placed on the other side chamber (see the scheme in Fig. 7B). The amount of time the test mouse spent investigating the stimuli was recorded during this social phase. As expected, WT mice spent more time within the social (novel mouse) side during the social phase compared with the non-social (novel object) side. On the contrary, KO mice during the social period spent less time within the social side and more time in the non-social side compared with WT mice (Fig. 7B). Therefore, the comparison of the time spent (in seconds, s) by WT and KO mice with the social stimulus resulted a significant difference (mean ± S.E.M., 378.42 ± 36.68 for WT; 275.70 ± 24.59 for KO; $P < 0.05$). Also the time spent by WT and KO mice with the novel object resulted a significant difference in the two

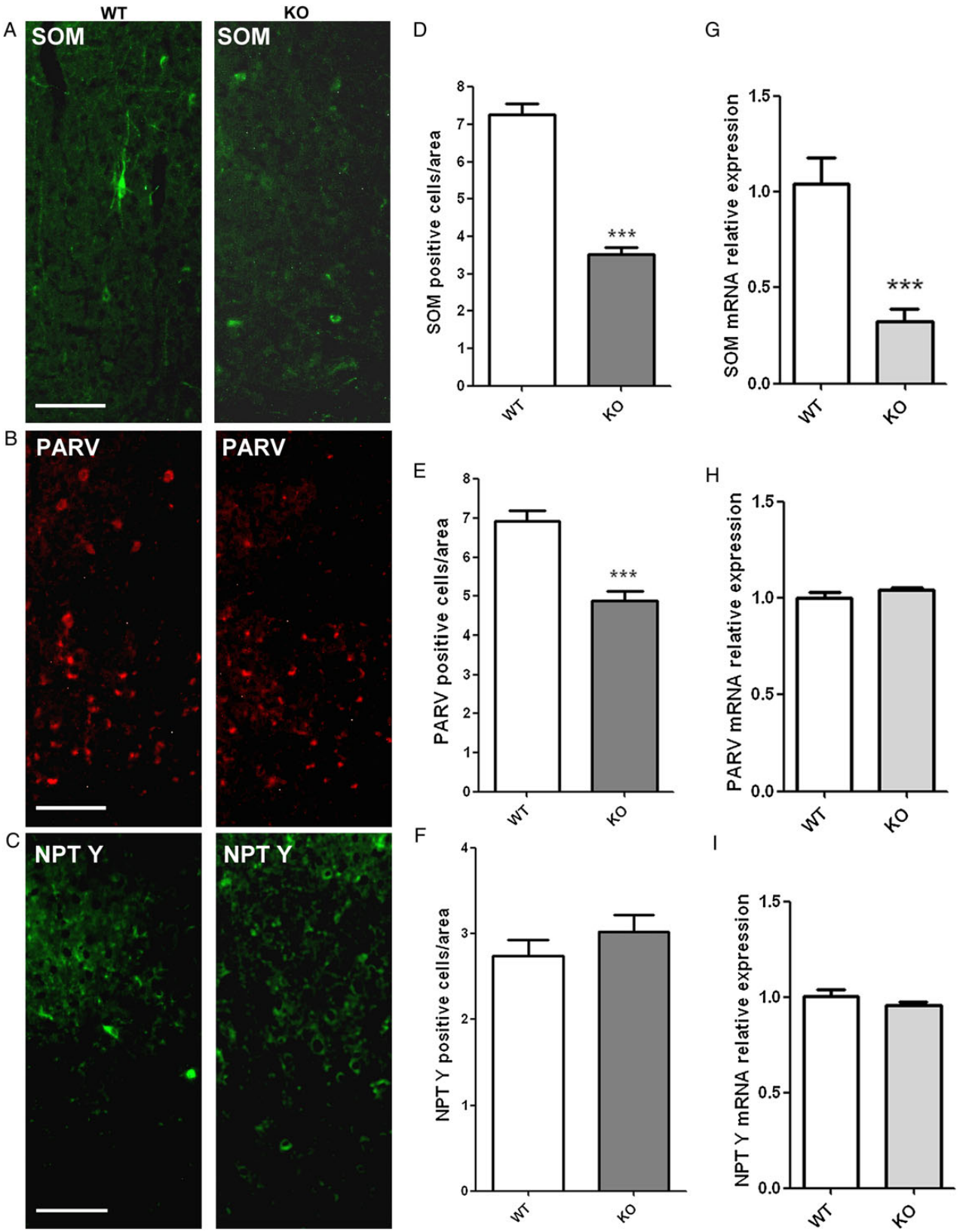

Figure 5. Reduced number of interneurons in adult KO mice SS cortex. Representative images of Somatostatin (SOM) (*A*), Parvalbumin (PARV) (*B*), and Neuropeptide Y (NPT Y) (*C*) positive cells in the SS cortex of WT (left) and KO (right) mice. Scale bar = 100 μm. Graphic representation of SOM^+ (*D*), $PARV^+$ (*E*), and NPT Y^+ (*F*) cells count per area in WT and KO mice SS cortex. Data show a significant decrease in SOM^+ and $PARV^+$ cells in KO compared with that in WT mice cortex. Data are expressed as mean ± S.E.M. ***$P < 0.0001$. (*G*,*H*,*I*) Graphic representation of QRT–PCR data obtained from RNA extracted from WT and KO SS cortex. Data are expressed as fold change of target gene (SOM in *G*, PARV in *H*, and NPT Y in *I*) expression in WT and KO cortex, normalized to the internal standard control gene (Actin). Only SOM showed a significant decrease in KO compared with WT mice (***$P = 0.0008$).

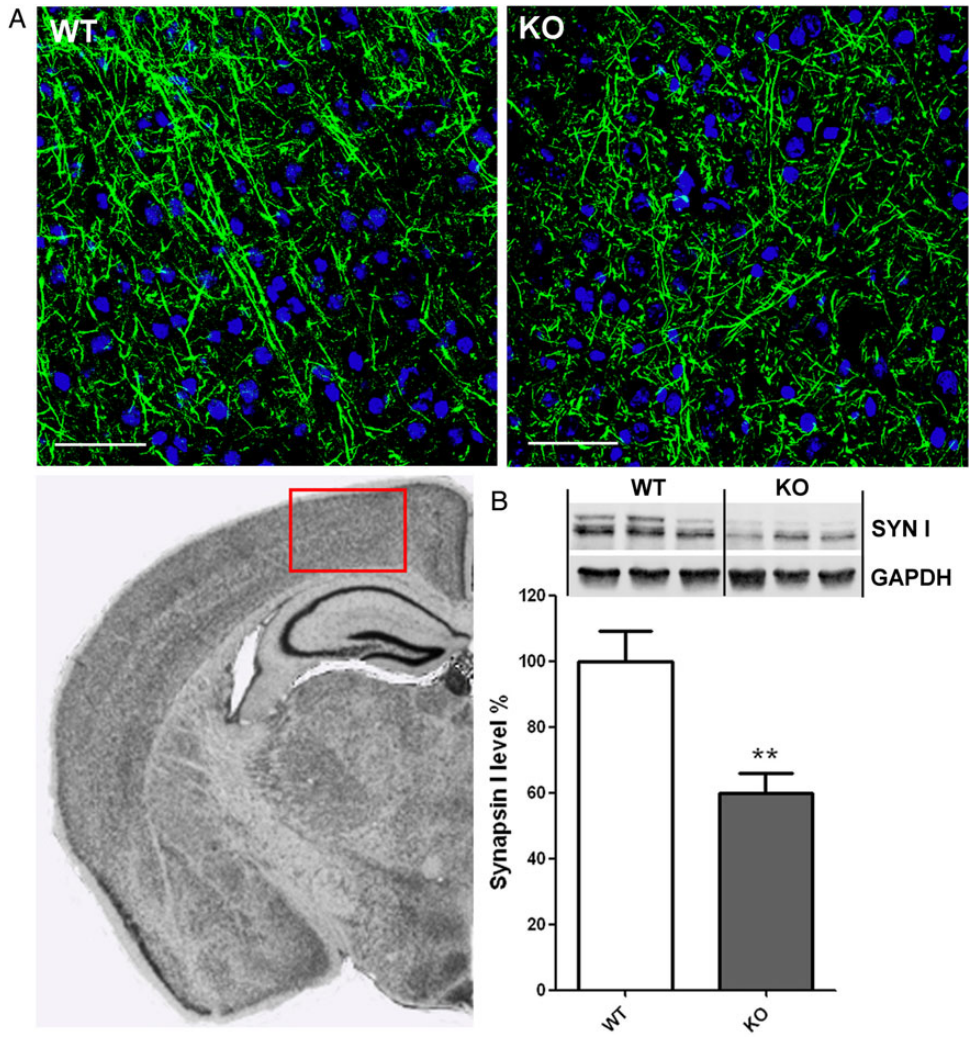

Figure 6. Altered neurite orientation in adult p50$^{-/-}$ mice SS cortex. Inset, scheme of an adult brain section with the indication (red marked area) of the cortical area of interest (corresponding to the somatosensory area). (*A*) Representative confocal images of anti-Neurofilament-200 (green) immunostaining on WT (left) and KO (right) brain slices of adult mice. DAPI staining is also present (blue). Pictures show an altered orientation of cortical neurites in KO cortex compared with that in WT mice. Scale bar = 50 µm. (*B*) Upper panel: representative immunoblot of WT and KO mice SS cortex lysates using anti-Synapsin I and anti-GAPDH antibodies. Graph: Graphic representation of Synapsin I protein levels analysis evaluated by western blot. Data are expressed as mean ± S.E.M., normalized for GAPDH. Synapsin I levels are significantly decreased in KO compared with WT SS cortex (**$P = 0.002$).

genotypes (mean ± S.E.M., 122.67 ± 29.99 for WT; 220.20 ± 32.08 for KO; $P < 0.05$). Indeed, WT mice dramatically preferred the novel mouse, while KO mice did not show any difference between novel object and novel mouse. A significant decrease was also observed in KO versus WT mice for the time spent sniffing the novel mouse (mean ± S.E.M., 137.92 ± 16.06 for WT; 78.90 ± 7.07 for KO; $P < 0.01$). Conversely, no difference was seen between genotypes in the amount of time spent in the center chamber (mean ± S.E.M., 98.92 ± 21.46 for WT; 104.10 ± 9.61 for KO; $P = 0.84$), in time spent grooming (mean ± S.E.M., 35.25 ± 9.61 for WT; 32.40 ± 6.25 for KO; $P = 0.81$), or in time spent sniffing novel object (mean ± S.E.M., 25.83 ± 5.69 for WT; 41.50 ± 7.83 for KO; $P = 0.11$). Finally, during the last 10 min of the test (phase IV), mice were tested for their performance in social recognition (or social memory) using the mouse known in the previous phase (familiar mouse) in the left chamber and a novel mouse (age- and genotype-matched intruder mouse) in the right chamber. No significant differences emerged between WT and KO mice.

Another test useful to analyze the social attitude in mice is the "reciprocal social interaction" test. It consists in the recording and subsequent analysis of the interaction during the 10 min duration test between the subject mouse and an age-, sex-, and strain-matched unfamiliar mouse (intruder subject) (Silverman et al. 2010; Scattoni et al. 2013) (see the scheme in Fig. 7C). We tested WT and p50$^{-/-}$ mice under this behavioral paradigm. The time spent doing the following actions was measured in the 10-min test: first contact latency, nose to nose sniffing, nose to anogenital sniffing, wrestling, following, mounting, pushing (all classified as "social activities"). Furthermore, exploring, self-grooming, and climbing were measured and evaluated as "non-social activities." As shown in Figure 7C, p50$^{-/-}$ mice spent significantly less time (expressed in seconds) in most social activities compared with WT (mean ± S.E.M., nose to nose sniffing 35.55 ± 4.58 for WT, 24.20 ± 1.94 for KO, $P < 0.05$; nose to anogenital sniffing 71.00 ± 11.79 for WT, 23.90 ± 3.36 for KO, $P < 0.005$; following 17.00 ± 3.29 for WT, 4.00 ± 1.65 for KO, $P <$

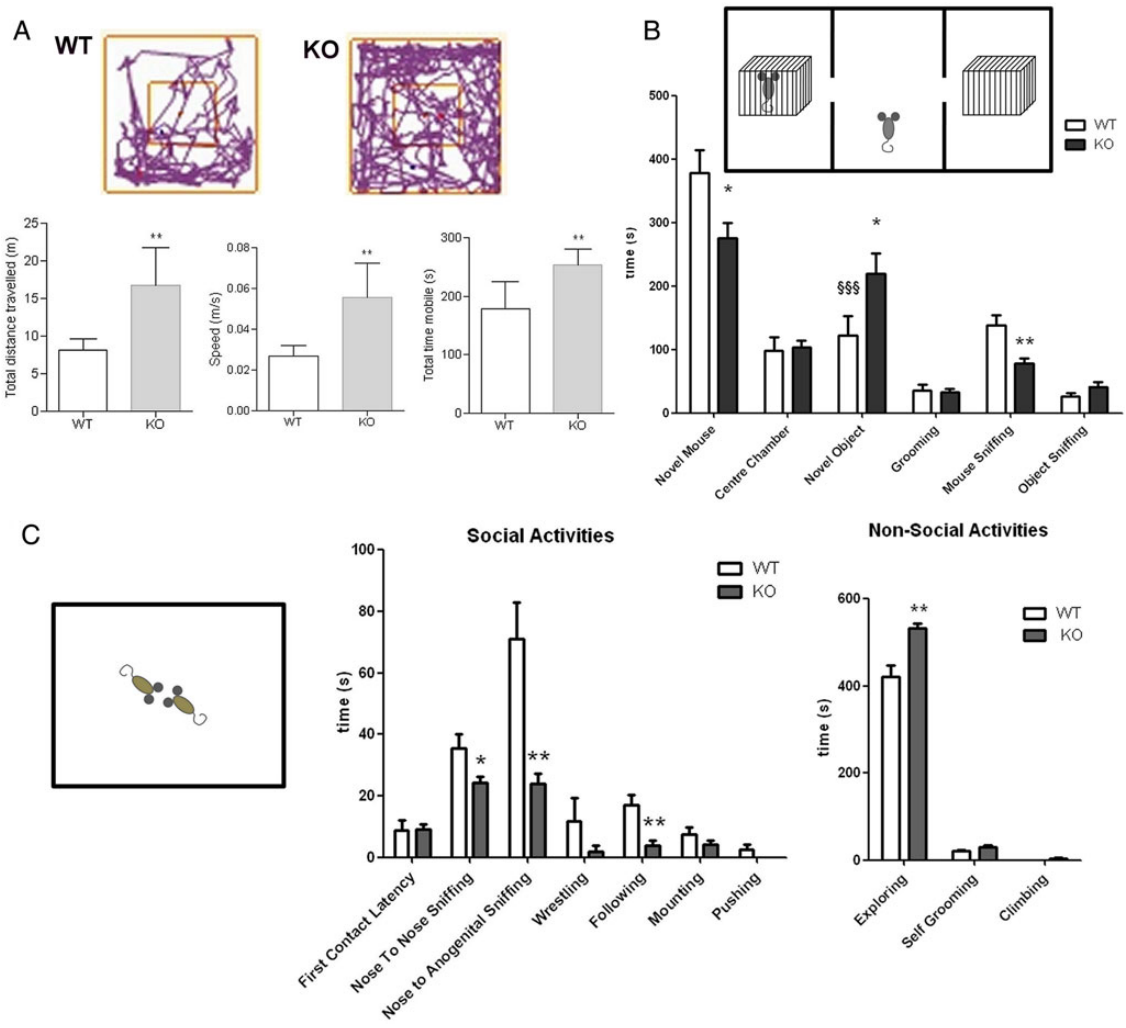

Figure 7. Increased activity and reduced social interaction in adult p50$^{-/-}$ mice. (*A*) In the inset, representative open field test layout performed by WT (left) and KO (right) mice; graphic representation of data collected in the open field test by automatically measuring the total distance travelled, the speed, and the total time mobile. Data show an increase in exploratory behavior and locomotor activity in KO compared with WT mice. $^{**}P < 0.01$ by *t*-test statistical analysis. (*B*) In the inset, schematic representation of the social approach test performed by means of the three-chambered apparatus. Graphic representation of data collected during the phase III (social phase) of the social approach test by measuring the time in seconds (s) spent by the subject mouse in staying with the novel mouse, in the center chamber, with the novel object, grooming, sniffing the mouse, and sniffing the object. Data show that KO mice spent less time with the novel mouse and more time with the novel object compared with the WT mice. $^{*}P < 0.05$; $^{**}P < 0.01$ by Two-way analysis of variance followed by the Bonferroni post-test analysis. WT mice significantly preferred the novel mouse, while KO mice did not show any difference between novel object and novel mouse. $^{§§§}P < 0.005$ by Two-way analysis of variance followed by the Sidak's multiple comparison test between novel mouse and novel object for WT. (*C*) On the left, schematic representation of the reciprocal social interaction test. Graphic representation of data collected during the reciprocal interaction test by measuring the time in seconds (s) spent by WT and KO mice in doing social (left) and non-social (right) activities. Data show that KO mice spent significantly less time, compared with the WT mice, in doing the following social activities: nose to nose sniffing, nose to anogenital sniffing, and following. $^{*}P < 0.05$, $^{**}P < 0.005$ by *t*-test statistical analysis. On the other hand, KO mice spent significantly more time, compared with WT mice, in exploring, a non-social activity. $^{**}P < 0.005$ by *t*-test statistical analysis. The KO mice are hyperactive, and their social attitude is reduced compared with the WT mice.

0.005). No significant differences were reported among genotypes in first contact latency (mean ± S.E.M., 8.82 ± 3.24 for WT, 9.00 ± 1.70 for KO; $P = 0.96$), wrestling (mean ± S.E.M., 11.91 ± 7.33 for WT, 2.00 ± 2.00 for KO; $P = 0.23$), mounting (mean ± S.E.M., 7.36 ± 2.49 for WT, 4.30 ± 1.09 for KO; $P = 0.29$), and pushing (mean ± S.E.M., 2.45 ± 1.68 for WT, 0 for KO; $P = 0.18$). Conversely, and in line with the increased activity in the open field, p50$^{-/-}$ mice spent more time (s) in a non-social activity such as exploring compared with the WT (mean ± S.E.M., 421.6 ± 26.41 for WT, 532.8 ± 11.08 for KO; $P < 0.005$). No differences were reported between genotypes in self-grooming (mean ± S.E.M., 20.64 ± 3.21 for WT, 29.20 ± 4.23 for KO; $P = 0.11$) and climbing (mean ± S.E.M., 0 for WT, 3.50 ± 2.53 for KO; $P = 0.16$).

Altogether, these data demonstrate that p50$^{-/-}$ mice display impaired social behavior and hyperactivity.

Risperidone Treatment Rescues Hyperactivity But Not Social Interaction Deficit in p50$^{-/-}$ Mice

An important goal in developing mouse models of neuropsychiatric diseases is to prove their predictive validity by testing treatments validated in human diseases. Risperidone is an atypical antipsychotic drug used to treat irritability in children and adolescents with neurodevelopmental disorders; it alleviates hyperactivity, repetitive behavior, aggression, and self-injurious behavior (McDougle et al. 2000, 2008). Risperidone was chosen

for the treatment, because it fits all the features requested: well-known and useful effect on management of behavioral problems such as irritability, hyperactivity, and repetitive behaviors, good safety, not disease-specific (Sharma and Shaw 2012). $p50^{-/-}$ mice and wild-type mice were treated with risperidone or vehicle both in acute and in chronic (21 days) regimen and then subjected to behavior tests. The acute treatment was used to set the dosage for the chronic treatment. Animals were treated with a wide dose range of risperidone (0.03, 0.06, 0.125, 0.5, 1 mg/kg) or with vehicle (0.9% NaCl). Thirty minutes after risperidone injection, mice were tested in the open field and the social approach test. As reported in Figure 8A, risperidone reduced, in a dose-dependent manner, distance travelled, speed, and total time mobile in KO mice. The lowest drug dose (0.03 mg/kg) was effective in reducing travelled distance (mean ± S.E.M., 12.43 ± 0.81 for vehicle and 6.96 ± 1.12 for 0.03 mg/kg risperidone; $P < 0.001$), speed (mean ± S.E.M., 0.045 ± 0.003 for vehicle and 0.023 ± 0.004 for 0.03 mg/kg; $P < 0.001$), and total time mobile (mean ± S.E.M., 227.1 ± 5.13 for vehicle and 138.0 ± 20.37 for 0.03 mg/kg risperidone; $P < 0.001$) in the open field test in KO mice. Conversely, only the highest drug dose (1 mg/kg) was effective in reducing travelled distance in WT mice (mean ± S.E.M., 8.41 ± 0.95 for vehicle and 2.04 ± 0.09 for 1 mg/kg risperidone; $P < 0.05$).

Risperidone acutely treated KO and WT mice were also tested in the reciprocal social interaction test. As shown in Figure 8B, risperidone failed to ameliorate defective social interaction in KO mice. Moreover, at highest doses (0.5–1 mg/kg), the drug decreased time spent in social activity and exploring both in WT and in KO mice, likely due to sedation (Aman et al. 2005; Kent et al. 2013). Based on data obtained in the acute treatment experiment, the dose of 0.3 mg/kg was chosen for chronic (21 days) oral administration of risperidone. Open field test data showed no significant effect in drug-treated compared with vehicle-treated WT mice, suggesting that the dose of 0.3 mg/kg was not sedative (Fig. 8C). Conversely, risperidone decreased activity of KO mice to WT levels, in terms of travelled distance (mean ± S.E.M., 17.84 ± 2.37 for vehicle and 7.58 ± 0.98 for 0.3 mg/kg risperidone; $P < 0.01$), speed (mean ± S.E.M., 0.060 ± 0.008 for vehicle and 0.025 ± 0.003 for 0.3 mg/kg risperidone; $P < 0.01$), and total time mobile (mean ± S.E.M., 252.40 ± 21.06 for vehicle and 147.30 ± 29.72 for 0.3 mg/kg risperidone; $P < 0.01$). Also under a chronic treatment regimen, risperidone was not able to ameliorate social attitude of KO mice, as demonstrated by no change in time spent in social activities in the reciprocal interaction test (Fig. 8D). Moreover, the drug did not reduce time spent exploring in KO as well as in WT mice, suggesting once again that the risperidone was not producing sedation. Concerning molecular targets, risperidone is a selective monoaminergic antagonist with high affinity for 5-HT_{2A} and dopaminergic D_2 receptors. Following risperidone treatment and behavioral test performance, mice were sacrificed and cortex mRNA extracts were used to analyze expression levels of dopamine D_2 and 5-HTR_{2A} receptors. We found that dopaminergic D_2 receptor (DRD2) mRNA level was significantly higher in the cortex of $p50^{-/-}$ compared with wild-type mice; risperidone treatment did not cause any significant change (mean ± S.E.M., 0.95 ± 0.14 for WT vehicle, 1.28 ± 0.19 for WT 0.3 mg/kg risperidone, 1.93 ± 0.38 for KO vehicle, 1.21 ± 0.16 for KO 0.3 mg/kg risperidone; $P < 0.05$ KO vehicle vs WT vehicle) (Fig. 9A). 5-HT_{2A} (HTR_{2A}) mRNA level did not show any significant difference between experimental groups analysed (mean ± S.E.M., 1.00 ± 0.13 for WT vehicle, 0.79 ± 0.03 for WT 0.3 mg/kg risperidone, 1.56 ± 0.23 for KO vehicle, 1.16 ± 0.10 for KO 0.3 mg/kg risperidone; $P = 0.051$ KO vehicle versus WT vehicle) (Fig. 9B). Finally, we performed an analysis of Synapsin I protein level by western blotting to measure the effect of risperidone on synaptic transmission. Synapsin I protein levels resulted significantly lower in cortex of $p50^{-/-}$ compared with wild-type mice. After risperidone treatment, no statistically significant change has been registered (mean ± S.E.M.: 123.3 ± 16.81 for WT vehicle, 69.87 ± 12.66 for KO vehicle, 114.10 ± 21.02 for WT 0.3 mg/kg risperidone, 104.10 ± 15.43 for KO 0.3 mg/kg risperidone; $P < 0.05$ for KO vehicle vs. WT vehicle).

Discussion

Based on the relevant role of NF-κB and Notch pathways during neurodevelopment, the aim of this study was to investigate the contribution of the p50 subunit on brain development and in particular on corticogenesis. For this reason, cortical cytoarchitecture of $p50^{-/-}$ and WT mice was extensively analysed.

At first, two proteins mainly involved in cortical cells migration were evaluated in both $p50^{-/-}$ and WT mice at P2: Reelin and BLBP. Reelin- and BLBP-expressing cells act as scaffold for migrating newborn neurons to reach their final cortical positioning. Although no difference emerged in protein localization pattern between genotypes, both Reelin protein levels and the number of BLBP-expressing cells resulted an increase for KO compared with WT mice. A close interrelation between Notch1, Reelin, and BLBP does exist. *Blbp* is a Notch1 target gene (Anthony et al. 2005), and a crosstalk between Reelin and Notch1 does exist and takes place during cortical cells migration to regulate laminar positioning (Hashimoto-Torii et al. 2008). Moreover, Reelin, via activation of Notch1 pathway, is necessary to induce BLBP expression and to promote process extension and maturation of the neural progenitors, the radial glial cells (Keilani and Sugaya 2008). Based on these observations, the increase in $BLBP^+$ cells and Reelin protein levels in $p50^{-/-}$ mice could correlate with Notch1 pathway hyperactivation previously demonstrated in these mutant mice (Bonini et al. 2011).

Subsequently, we carefully analysed WT and KO mice cortical layering. Immunohistochemistry with layer-specific markers was performed on P2 mice brain, using anti-Cux1 (for layers III–II) and anti-Ctip2 (for Layers VI–V) antibodies. Cux1- and Ctip2-positive cells were similarly positioned in WT and KO mice cortex, with Cux1 staining the outer and Ctip2 the deeper cortical layers. However, quantitative measurement of the Cux1- and Ctip2-positive layers revealed an increased thickness of Ctip2-positive layer in KO compared with that in WT mice cortex. Layers V–VI are composed of corticospinal motor neurons, related subcerebral projecting neurons, and corticothalamic neurons. Furthermore, CTIP2 plays a critical role during axonal extension and pathfinding by subcerebral projecting neurons of the cerebral cortex (Arlotta et al. 2005). Based on these findings, an increase in Ctip2-expressing cell layer may represent, other than a difference in cortical layering between WT and KO mice, an alteration in cortex-subcortical target innervations. The increase of this specific layer thickness reflects also on an overall cortical thickness increase in KO compared with WT mice.

We then investigated whether alterations during neurodevelopment could have caused persistent abnormalities in the cytoarchitecture of $p50^{-/-}$ mice cortex. To this aim, we performed a detailed analysis of minicolumns in WT and $p50^{-/-}$ adult mice. Minicolumns alterations (minicolumnopathies) have been linked to various psychiatric disorders, including autism and schizophrenia (Beasley et al. 2005; Buxhoeveden et al. 2006; Casanova et al. 2006). We focused our study in the somatosensory (SS) cortex due to the fact that in previous studies we found an increased and altered expression pattern of both Notch1 receptor and its

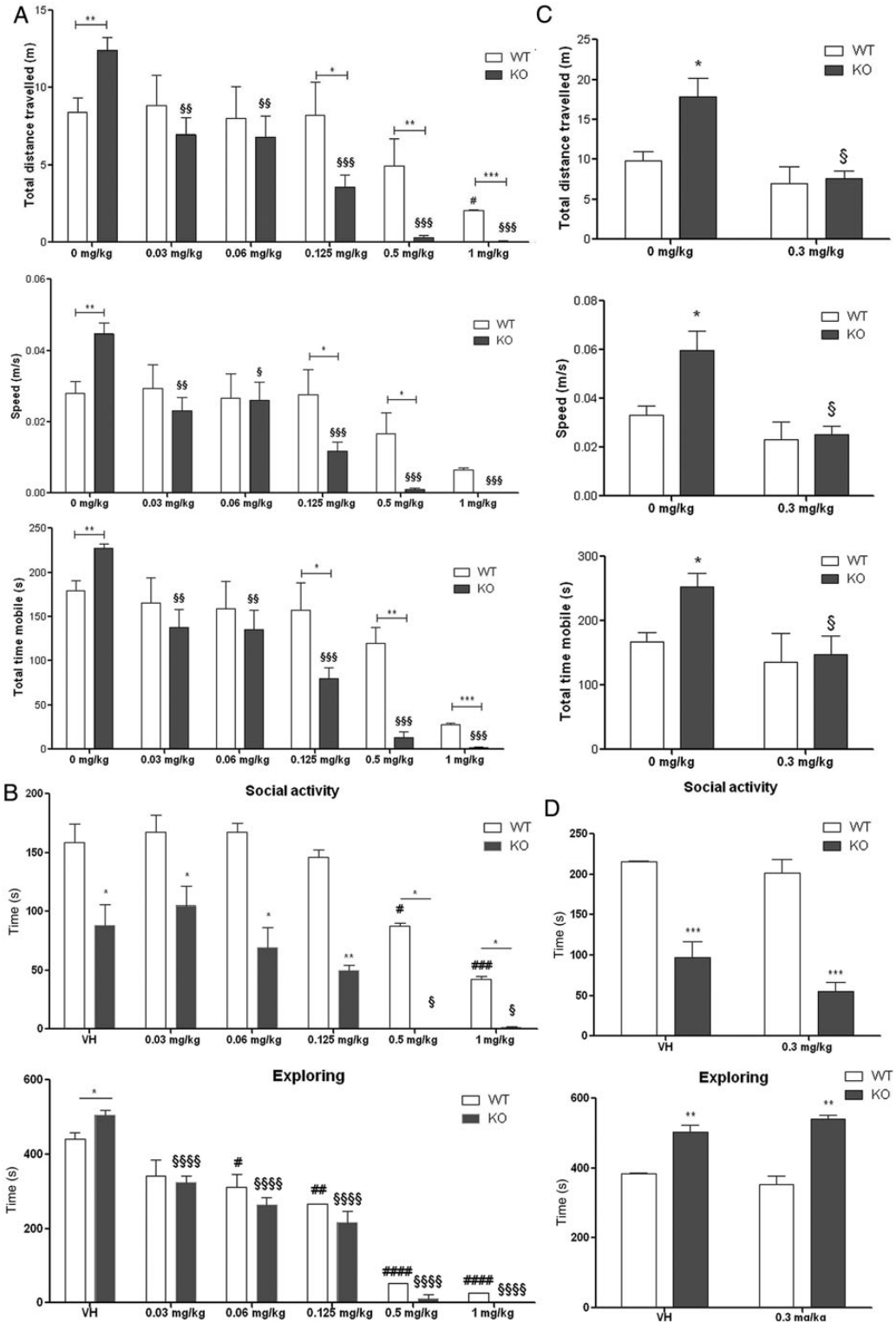

Figure 8. Risperidone treatment rescues hyperactivity but not social interaction deficit in p50$^{-/-}$ mice. (*A*) Graphic representation of data collected in the open field test on mice treated acutely with risperidone, at indicated doses, or vehicle (VH). Distance travelled, speed, and total time mobile are reported. Data show that acute risperidone treatment, compared with vehicle, decreases activity in KO mice. (*B*) Graphic representation of data collected in the reciprocal social interaction test on mice treated acutely with risperidone, at different doses, or vehicle. Social activity and exploring are reported. Data show that acute risperidone treatment, although effective in reducing exploring, does not ameliorate social activity in KO mice, while exhibiting sedative effects both in WT and in KO mice at highest doses (0.5 and 1 mg/kg). (*C*) Graphic representation of data collected in the open field test on mice chronically treated with risperidone 0.3 mg/kg. Distance travelled, speed, and total time mobile are reported. Data show that chronic risperidone treatment decreases activity in KO mice, compared with vehicle. (*D*) Graphic representation of data collected in the reciprocal social interaction test on mice chronically treated with risperidone (0.3 mg/kg). Social activity and exploring are reported. Data show that chronic risperidone treatment does not ameliorate the social activity in KO mice. §treated KO versus vehicle KO. *KO versus WT. $^{\#}$treated WT versus vehicle WT. $^{§}P < 0.01$, $^{§§}P < 0.001$, $^{§§§}P < 0.0001$ by One-way analysis of variance and Dunnett's multiple comparison test. $^{\#}P < 0.05$ by One-way analysis of variance and Dunnett's multiple comparison test. $^{*}P < 0.05$, $^{**}P < 0.005$, $^{***}P < 0.0005$ by *t*-test analysis.

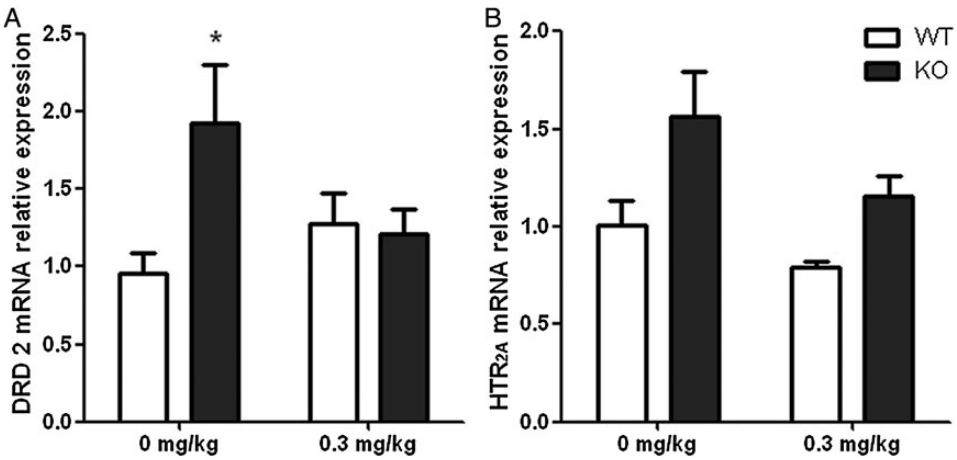

Figure 9. DRD2 and HTR_{2A} expression level analysis after risperidone treatment. Graphic representation of QRT–PCR data obtained from RNA extracted from wild-type (WT) and $p50^{-/-}$ (KO) mice cortex after chronic treatment with risperidone 0.3 mg/kg. Data are expressed as fold change of target gene expression in WT and KO cortex, normalized to the internal standard control gene (actin). (*A*) Analysis of dopaminergic D_2 receptor (DRD2) expression. (*B*) Analysis of 5-HT_{2A} (HTR_{2A}) receptor expression. *$P < 0.05$ by One-way analysis of variance and Bonferroni's multiple comparison test (KO vs. WT).

ligand Jagged1 in such area of KO mice cortex at P1 (Bonini et al. 2011). Minicolumns were studied also in the cingulated cortex, more specifically the cingulated gyrus (CG), an area that has been involved in motivation, important aspect in disorders such as depression and schizophrenia (Adams and David 2007; Drevets et al. 2008). No overt anatomical and structural alterations are apparent between WT and KO mice, concerning brain size and cortical thickness. By employing a previously published methodology (Buxhoeveden et al. 2000; Srivastava et al. 2012), several differences were demonstrated in $p50^{-/-}$ SS cortex minicolumnar structure compared with WT mice. In particular, mutant mice displayed: 1) an increase in cell density per column (both total cells and pyramidal neurons); 2) a decrease in cell spacing; 3) an increase in TPLR, a measurement of linearity of cell column. These findings are quite interesting since it has been suggested that alterations of any of these parameters can affect minicolumnar function and subsequently alter local and regional brain functions (Casanova and Tillquist 2008). Moreover, these changes were specific for the SS cortex of $p50^{-/-}$ mice, since no significant difference was observed between genotypes in CG.

To better understand the possible structural and functional effects of the increase in cell density found in SS cortex of KO compared with that of WT mice, we investigated whether changes affected specific cellular phenotype in the SS cortex. Our results suggest that the increase in cell density is not consequent to a specific cell population increase, but rather involves several cell types, including neurons, glia, and interneurons, as demonstrated by data on the protein levels obtained by using markers for neurons (NeuN), astrocytes (GFAP), and GABAergic neurons (GAD65 and GAD67). Data from quantitative RT–PCR did not display difference between WT and KO mRNA expression of cell markers analysed suggesting that the observed differences between $p50^{-/-}$ and WT mice were not associated with changes in transcriptional activity. Several studies clearly indicate that defective development of GABAergic neurons and the resulting reduced inhibition, might contribute to the pathogenesis of psychiatric disorders (Gogolla et al. 2009; Chao et al. 2010). To verify whether alterations in interneuron number were also present in $p50^{-/-}$ mice, we investigated the expression profile of some GABAergic interneurons in the SS cortex of WT and KO mice by using quantitative RT–PCR and immunohistochemistry for interneuron-specific markers. We found that both SOM- and PARV-expressing interneurons, but not NPT Y-expressing neurons, were reduced in SS cortex of KO compared with WT mice, suggesting that despite cell density increase in the SS cortex of KO mice, specific classes of interneurons were reduced. It is well-known that PARV- and SOM-positive interneurons target distinct compartments on pyramidal cells, the first ones providing perisomatic inhibition, and the second ones forming synapses onto dendrites (Markram et al. 2004; Ascoli et al. 2008). These data suggest that KO mice, compared with their WT counterpart, may potentially display imbalance in neuronal excitatory/inhibitory circuits in their SS cortex.

Furthermore, to go deeper into the neuronal network analysis, we investigated neurons branching and synaptic net connections in cortical tissue by performing immunohistochemistry with an anti-Neurofilament-200 antibody and evaluating Synapsin I levels by western blot in both mouse genotypes. It emerged that KO mice display alterations in cortical neurons neurite orientation in the SS cortex, and in particular that they lack organized radial orientation, from basal to apical cortical layers, as observed in WT mice SS cortex. Moreover, Synapsin I levels resulted a significant decrease for KO SS cortex compared with WT. Since all synapses of both glutamatergic and GABAergic neurons of mouse somatosensory cortex are virtually recognized by anti-Synapsin I antibody (Micheva et al. 2010), these data suggest that KO mice, despite an increased cell density, are characterized by a general loss of synaptic connections in this cortical area. These data, together with the alterations in columnar structure, suggest a loss of organization of neuronal circuits in the somatosensory cortex of $p50^{-/-}$ mice.

To study whether these alterations could reflect on animal behavior, we tested both WT and $p50^{-/-}$ mice in the open field test, to evaluate their locomotion and exploratory activity. As previously described (Kassed and Herkenham 2004), $p50^{-/-}$ mice showed increased exploratory behavior compared with WT animals, confirming a hyperactivity of $p50^{-/-}$ compared with WT mice. Then, we tested $p50^{-/-}$ mice for social attitude, since similar cortical structural alterations have been previously reported in mouse models with social impairment (Srivastava et al. 2012; Sgadò et al. 2013). We chose the reciprocal social interaction and the social approach tests, that are well approved and validated tests important to analyze the social attitude (a focal aspect of some neurodevelopmental disorders, such as autism) of $p50^{-/-}$ mice (Silverman et al. 2010).

Surprisingly, the social approach test revealed a significant reduction in social interest of $p50^{-/-}$ compared with WT mice. Moreover, the reciprocal social interaction test revealed a decrease in time spent in social activities and an increase in time spent in non-social activities in $p50^{-/-}$ compared with WT mice. Hence, the effect of risperidone, an antipsychotic drug commonly used to treat irritability in neurodevelopmental disorders, was analysed on mice motility and social behavior. The drug, both under acute and chronic treatment, could effectively reduce hyperactivity in $p50^{-/-}$ mice with no effects in WT mice except for the highest sedative dose when given acutely. Conversely, no ameliorating effect was observed after risperidone treatment on social behavior in mutant mice.

The perspective concerning the developmental disposition of minicolumns and subsequent effects regarding hierarchical brain networks has implications for many psychiatric conditions, such as autism, schizophrenia, and epilepsy (Casanova and Tillquist 2008). Moreover, Casanova et al. (2002) reported that the neurological substrate of autism lies in increased proliferation of radial glia progenitors and subsequent increase in minicolumnar numbers. Interestingly, using whole-exome sequencing data, Poultney et al. (2013) identified disruption of small exonic copy number variation in autism genes, and p50 was found to be altered. Other studies also correlate NF-κB pathway with the pathogenesis of schizophrenia (Song et al. 2009; Chen et al. 2014).

In summary, our data led us to conclude that the lack of NF-κB p50 subunit, potentially via dysregulation of other key neurodevelopmental pathways such as Notch1, is associated with SS cortex-specific and peculiar structural changes and behavioral abnormalities in social interaction. Our studies also point to potential links between altered function of NF-κB pathway and the pathogenesis of neurodevelopmental disorders.

Funding

This work was supported by Fondazione Cariplo - New Opportunities and Ways towards ERC (NOW ERC) (grant number: 2014-2256) and Research Grant from the University of Brescia (grant number: EX60%2015MEMO). Funding to pay the Open Access publication charges for this article was provided by Fondazione Cariplo - New Opportunities and Ways towards ERC (NOW ERC) (grant number: 2014-2256).

Notes

Conflict of Interest: None declared.

References

Adams R, David AS. 2007. Patterns of anterior cingulate activation in schizophrenia: a selective review. Neuropsychiatr Dis Treat. 3:87–101.

Aman MG, Arnold LE, McDougle CJ, Vitiello B, Scahill L, Davies M, McCracken JT, Tierney E, Nash PL, Posey DJ, et al. 2005. Acute and long-term safety and tolerability of risperidone in children with autism. J Child Adolesc Psychopharmacol. 15:869–884.

Amodeo DA, Jones JH, Sweeney JA, Ragozzino ME. 2014. Risperidone and the 5-HT2A receptor antagonist M100907 improve probabilistic reversal learning in BTBR T + tf/J mice. Autism Res. 7:555–567.

Ang HL, Tergaonkar V. 2007. Notch and NFkappaB signaling pathways: do they collaborate in normal vertebrate brain development and function? Bioessays. 29:1039–1047.

Anthony TE, Mason HA, Gridley T, Fishell G, Heintz N. 2005. Brain lipid-binding protein is a direct target of Notch signaling in radial glial cells. Genes Dev. 19:1028–1033.

Arlotta P, Molyneaux BJ, Chen J, Inoue J, Kominami R, Macklis JD. 2005. Neuronal subtype-specific genes that control corticospinal motor neuron development in vivo. Neuron. 45:207–221.

Ascoli GA, Alonso-Nanclares L, Anderson SA, Barrionuevo G, Benavides-Piccione R, Burkhalter A, Buzsáki G, Cauli B, Defelipe J, Fairén A, et al. 2008. Petilla terminology: nomenclature of features of GABAergic interneurons of the cerebral cortex. Nat Rev Neurosci. 9:557–568.

Beasley CL, Chana G, Honavar M, Landau S, Everall IP, Cotter D. 2005. Evidence for altered neuronal organisation within the planumtemporale in major psychiatric disorders. Schizophr Res. 73:69–78.

Bonini SA, Ferrari-Toninelli G, Uberti D, Montinaro M, Buizza L, Lanni C, Grilli M, Memo M. 2011. Nuclear factor κB-dependent neurite remodeling is mediated by Notch pathway. J Neurosci. 31:11697–11705.

Breunig JJ, Silbereis J, Vaccarino FM, Sestan N, Rakic P. 2007. Notch regulates cell fate and dendrite morphology of newborn neurons in the postnatal dentate gyrus. Proc Natl Acad Sci USA. 104:20558–20563.

Buxhoeveden DP, Semendeferi K, Buckwalter J, Schenker N, Switzer R, Courchesne E. 2006. Reduced minicolumns in the frontal cortex of patients with autism. Neuropathol Appl Neurobiol. 32:483–491.

Buxhoeveden DP, Switala AE, Roy E, Casanova MF. 2000. Quantitative analysis of cell columns in the cerebral cortex. J Neurosci Methods. 97:7–17.

Cao Q, Li P, Lu J, Dheen ST, Kaur C, Ling EA. 2010. Nuclear factor-κB/p65 responds to changes in the Notch signaling pathway in murine BV-2 cells and in amoeboid microglia in postnatal rats treated with the γ-secretase complex blocker DAPT. J Neurosci Res. 88:2701–2714.

Casanova MF, Buxhoeveden DP, Switala AE, Roy E. 2002. Minicolumnar pathology in autism. Neurology. 58:428–432.

Casanova MF, Tillquist CR. 2008. Encephalization, emergent properties, and psychiatry: a minicolumnar perspective. Neuroscientist. 14:101–118.

Casanova MF, van Kooten IA, Switala AE, van Engeland H, Heinsen H, Steinbusch HW, Hof PR, Trippe J, Stone J, Schmitz C. 2006. Minicolumnar abnormalities in autism. Acta Neuropathol. 112:287–303.

Caviness VS Jr, Rakic P. 1978. Mechanisms of cortical development: a view from mutations in mice. Annu Rev Neurosci. 1:297–326.

Cesca F, Baldelli P, Valtorta F, Benfenati F. 2010. The synapsins: key actors of synapse function and plasticity. Prog Neurobiol. 91:313–348.

Chao HT, Chen H, Samaco RC, Xue M, Chahrour M, Yoo J, Neul JL, Gong S, Lu HC, Heintz N, et al. 2010. Dysfunction in GABA signalling mediates autism-like stereotypies and Rett syndrome phenotypes. Nature. 468:263–269.

Chen B, Schaevitz LR, McConnell SK. 2005. Fezl regulates the differentiation and axon targeting of layer 5 subcortical projection neurons in cerebral cortex. Proc Natl Acad Sci USA. 102:17184–17189.

Chen B, Wang SS, Hattox AM, Rayburn H, Nelson SB, McConnell SK. 2008. The Fezf2-Ctip2 genetic pathway regulates the fate choice of subcortical projection neurons in the developing cerebral cortex. Proc Natl Acad Sci USA. 105:11382–11387.

Chen SF, Chao YL, Shen YC, Chen CH, Weng CF. 2014. Resequencing and associationstudy of the NFKB activating protein-like gene (NKAPL) in schizophrenia. Schizophr Res. 157:169–174.

Cubelos B, Sebastián-Serrano A, Beccari L, Calcagnotto ME, Cisneros E, Kim S, Dopazo A, Alvarez-Dolado M, Redondo JM, Bovolenta P, et al. 2010. Cux1 and Cux2 regulate dendritic branching, spine morphology, and synapses of the upper layer neurons of the cortex. Neuron. 66:523–535.

D'Arcangelo G, Miao GG, Chen SC, Soares HD, Morgan JI, Curran T. 1995. A protein related to extracellular matrix proteins deleted in the mouse mutant reeler. Nature. 374:719–723.

De Camilli P, Cameron R, Greengard P. 1983. Synapsin I (protein I), a nerveterminal-specific phosphoprotein. I. Its general distribution in synapses of the central and peripheral nervous system demonstrated by immunofluorescence infrozen and plastic sections. J Cell Biol. 96:1337–1354.

Denis-Donini S, Dellarole A, Crociara P, Francese MT, Bortolotto V, Quadrato G, Canonico PL, Orsetti M, Ghi P, Memo M, et al. 2008. Impaired adult neurogenesis associated with short-term memory defects in NF-kappaB p50-deficient mice. J Neurosci. 28:3911–3919.

Drevets WC, Savitz J, Trimble M. 2008. The subgenual anterior cingulate cortex in mood disorders. CNS Spectr. 13:663–681.

Fassio A, Raimondi A, Lignani G, Benfenati F, Baldelli P. 2011. Synapsins: from synapse to network hyperexcitability and epilepsy. Semin Cell Dev Biol. 22:408–415.

Feng L, Hatten ME, Heintz N. 1994. Brain lipid-binding protein (BLBP): a novel signaling system in the developing mammalian CNS. Neuron. 12:895–908.

Gaiano N. 2008. Strange bedfellows: reelin and Notch signaling interact to regulate cell migration in the developing neocortex. Neuron. 60:189–191.

Gogolla N, Leblanc JJ, Quast KB, Südhof TC, Fagiolini M, Hensch TK. 2009. Common circuit defect of excitatory-inhibitory balance in mouse models of autism. J Neurodev Disord. 1:172–181.

Gaiano N, Nye JS, Fishell G. 2000. Radial glial identity is promoted by Notch1 signaling in the murine forebrain. Neuron. 26:395–404.

Gould GG, Hensler JG, Burke TF, Benno RH, Onaivi ES, Daws LC. 2011. Density and function of central serotonin (5-HT) transporters, 5-HT1A and 5-HT2A receptors, and effects of their targeting on BTBR T+tf/J mouse social behavior. J Neurochem. 116:291–303.

Grilli M, Memo M. 1999. Nuclear factor-kappaB/Rel proteins: a point of convergence of signalling pathways relevant in neuronal function and dysfunction. Biochem Pharmacol. 57:1–7.

Hartfuss E, Galli R, Heins N, Götz M. 2001. Characterization of CNS precursor subtypes and radial glia. Dev Biol. 229:15–30.

Hartfuss E, Förster E, Bock HH, Hack MA, Leprince P, Luque JM, Herz J, Frotscher M, Götz M. 2003. Reelin signaling directly affects radial glia morphology and biochemical maturation. Development. 130:4597–4609.

Hashimoto-Torii K, Torii M, Sarkisian MR, Bartley CM, Shen J, Radtke F, Gridley T, Sestan N, Rakic P. 2008. Interaction between Reelin and Notch signaling regulates neuronal migration in the cerebral cortex. Neuron. 60:273–284.

Hevner RF. 2007. Layer-specific markers as probes for neuron type identity in human neocortex and malformations of cortical development. J Neuropathol Exp Neurol. 66:101–109.

Kassed CA, Herkenham M. 2004. NF-kappaB p50-deficient mice show reduced anxiety-like behaviors in tests of exploratory drive and anxiety. Behav Brain Res. 154:577–584.

Kassed CA, Willing AE, Garbuzova-Davis S, Sanberg PR, Pennypacker KR. 2002. Lack of NF-kappaB p50 exacerbates degeneration of hippocampal neurons after chemical exposure and impairs learning. Exp Neurol. 176:277–288.

Keilani S, Sugaya K. 2008. Reelin induces a radial glial phenotype in human neural progenitor cells by activation of Notch-1. BMC Dev Biol. 8:69.

Kent JM, Hough D, Singh J, Karcher K, Pandina G. 2013. An open-label extension study of the safety and efficacy of risperidone in children and adolescents with autistic disorder. J Child Adolesc Psychopharmacol. 23:676–686.

Kovács AD, Chakraborty-Sett S, Ramirez SH, Sniderhan LF, Williamson AL, Maggirwar SB. 2004. Mechanism of NF-kappaB inactivation induced by survival signal withdrawal in cerebellar granule neurons. Eur J Neurosci. 20:345–352.

Kucharczak J, Simmons MJ, Fan Y, Gélinas C. 2003. To be, or not to be: NF-kappaB is the answer–role of Rel/NF-kappaB in the regulation of apoptosis. Oncogene. 22:8961–8982.

Lasky JL, Wu H. 2005. Notch signaling, brain development, and human disease. Pediatr Res. 57:104R–109R.

Markram H, Toledo-Rodriguez M, Wang Y, Gupta A, Silberberg G, Wu C. 2004. Interneurons of the neocortical inhibitory system. Nat Rev Neurosci. 5:793–807.

Marin-Padilla M. 1978. Dual origin of the mammalian neocortex and evolution of the cortical plate. Anat Embryol (Berl). 152:109–126.

Mason HA, Rakowiecki SM, Gridley T, Fishell G. 2006. Loss of notch activity in the developing central nervous system leads to increased cell death. Dev Neurosci. 28:49–57.

McDougle CJ, Scahill L, McCracken JT, Aman MG, Tierney E, Arnold LE, Freeman BJ, Martin A, McGough JJ, Cronin P, et al. 2000. Research units on pediatric psychopharmacology (RUPP) autism network.background and rationale for an initial controlled study of risperidone. Child Adolesc Psychiatr Clin N Am. 9:201–224.

McDougle CJ, Stigler KA, Erickson CA, Posey DJ. 2008. Atypical antipsychotics in children and adolescents with autistic and other pervasive developmentaldisorders. J Clin Psychiatry. 69:15–20.

Methot L, Hermann R, Tang Y, Lo R, Al-Jehani H, Jhas S, Svoboda D, Slack RS, Barker PA, Stifani S. 2013. Interaction and antagonistic roles of NF-κB and Hes6 in the regulation of cortical neurogenesis. Mol Cell Biol. 33:2797–2808.

Micheva KD, Busse B, Weiler NC, O'Rourke N, Smith SJ. 2010. Single-synapse analysis of a diverse synapse population: proteomic imaging methods and markers. Neuron. 68:639–653.

Molyneaux BJ, Arlotta P, Menezes JR, Macklis JD. 2007. Neuronal subtype specification in the cerebral cortex. Nat Rev Neurosci. 8:427–437.

Moon HM, Wynshaw-Boris A. 2013. Cytoskeleton in action: lissencephaly, a neuronal migration disorder. Wiley Interdiscip Rev Dev Biol. 2:229–245.

Mountcastle VB. 1997. The columnar organization of the neocortex. Brain. 120:701–722.

Mountcastle VB. 1957. Modality and topographic properties of single neurons of cat's somatic sensory cortex. J Neurophysiol. 20:408–434.

Munji RN, Choe Y, Li G, Siegenthaler JA, Pleasure SJ. 2011. Wnt signaling regulates neuronal differentiation of cortical intermediate progenitors. J Neurosci. 31:1676–1687.

Osipo C, Golde TE, Osborne BA, Miele LA. 2008. Off the beaten pathway: the complex cross talk between Notch and NF-kappaB. Lab Invest. 88:11–17.

Poultney CS, Goldberg AP, Drapeau E, Kou Y, Harony-Nicolas H, Kajiwara Y, De Rubeis S, Durand S, Stevens C, Rehnström K, et al. 2013. Identification of small exonic CNV from whole-

exome sequence data and application to autism spectrum disorder. Am J Hum Genet. 93:607–619.
Rakic P. 1988. Defects of neuronal migration and the pathogenesis of cortical malformations. Prog Brain Res. 73:15–37.
Rozen S, Skaletsky H. 2000. Primer3 on the WWW for general users and for biologist programmers. Methods Mol Biol. 132:365–386.
Scattoni ML, Martire A, Cartocci G, Ferrante A, Ricceri L. 2013. Reduced social interaction, behavioural flexibility and BDNF signalling in the BTBR T + tf/J strain, a mouse model of autism. Behav Brain Res. 251:35–40.
Sgadò P, Genovesi S, Kalinovsky A, Zunino G, Macchi F, Allegra M, Murenu E, Provenzano G, Tripathi PP, Casarosa S, et al. 2013. Loss of GABAergic neurons in the hippocampus and cerebral cortex of Engrailed-2 null mutant mice: implications for autism spectrum disorders. Exp Neurol. 247:496–505.
Sha WC, Liou HC, Tuomanen EI, Baltimore D. 1995. Targeted disruption of the p50 subunit of NF-kappa B leads to multifocal defects in immune responses. Cell. 80:321–330.
Sharma A, Shaw SR. 2012. Efficacy of risperidone in managing maladaptive behaviors for children with autistic spectrum disorder: a meta-analysis. J Pediatr Health Care. 26:291–299.
Sholl DA. 1953. Dendritic organization in the neurons of the visual and motor cortices of the cat. J Anat. 87:387–406.
Silverman JL, Yang M, Lord C, Crawley JN. 2010. Behavioural phenotyping assays for mouse models of autism. Nat Rev Neurosci. 11:490–502.
Song XQ, Lv LX, Li WQ, Hao YH, Zhao JP. 2009. The interaction of nuclearfactor-kappa B and cytokines is associated with schizophrenia. Biol Psychiatry. 65:481–488.
Srivastava DP, Jones KA, Woolfrey KM, Burgdorf J, Russell TA, Kalmbach A, Lee H, Yang C, Bradberry MM, Wokosin D, et al. 2012. Social, communication, and cortical structural impairments in Epac2-deficient mice. J Neurosci. 32: 11864–11878.
Widera D, Mikenberg I, Kaltschmidt B, Kaltschmidt C. 2006. Potential role of NF-kappaB in adult neural stem cells: the underrated steersman? Int J Dev Neurosci. 24:91–102.
Yang M, Silverman JL, Crawley JN. 2011. Automated three-chambered social approach task for mice. Curr Protoc Neurosci. Chapter 8. Unit 8.26. Supplement 56. p 8.26.1-8.26.16.
Yoon K, Gaiano N. 2005. Notch signaling in the mammalian central nervous system: insights from mouse mutants. Nat Neurosci. 8:709–715.
Yoon KJ, Koo BK, Im SK, Jeong HW, Ghim J, Kwon MC, Moon JS, Miyata T, Kong YY. 2008. Mind bomb 1-expressing intermediate progenitors generate notch signaling to maintain radial glial cells. Neuron. 58:519–531.